Inorganica Chimica Acta 399 (2013) 19–35

Contents lists available at SciVerse ScienceDirect

Inorganica Chimica Acta

journal homepage: www.elsevier.com/locate/ica

Synthesis, crystal structures, molecular simulations for hydrogen gas adsorption, fluorescent and antimicrobial properties of pyrazine-2,3-dicarboxylate complexes

Güneş Günay [a], Okan Zafer Yeşilel [a,*], Cihan Darcan [b], Seda Keskin [c], Orhan Büyükgüngör [d]

[a] Eskişehir Osmangazi University, Faculty of Arts and Sciences, Department of Chemistry, 26480 Eskişehir, Turkey
[b] Bilecik Şeyh Edebali University, Faculty of Arts and Sciences, Department of Molecular Biology and Genetics, Gülümbe, 11000 Bilecik, Turkey
[c] Koç University, Department of Chemical and Biological Engineering, İstanbul, Turkey
[d] Ondokuz Mayıs University, Faculty of Arts and Sciences, Department of Physics, 55139 Samsun, Turkey

ARTICLE INFO

Article history:
Received 21 September 2012
Received in revised form 19 December 2012
Accepted 23 December 2012
Available online 10 January 2013

Keywords:
Coordination polymers
Pyrazine-2,3-dicarboxylate complexes
Imidazole complexes
Hydrogen gas adsorption, Solvent effect
Antimicrobial activities

ABSTRACT

Eight new pyrazine-2,3-dicarboxylate complexes have been synthesized and structurally characterized. The pzdc ligand bridges two neighboring metal atoms to form a 1D chain in complexes **1**, **3–8**. The structure of the complex **2** is mononuclear. It is noted that when dimethylformamide was replaced by methanol, a 1-D double-chain structure of **3** was formed instead of the mononuclear structure of **2**. The most interesting feature of **3** is the presence of C–H···Cu close hydrogen bonding interactions. In complexes, the pzdc ligand exhibits four kinds of coordination modes. The adjacent chains are held together by hydrogen bonds, C–H···π and π···π interactions, forming three-dimensional network. Complexes **4–8** exhibit strong fluorescent emission bands in the solid state at room temperature. Atomically detailed simulations were used to assess the potential of complexes in gas storage applications. Complexes **2** and **7** have showed antimicrobial activity on studied microorganisms.

1. Introduction

The rational design and construction of coordination polymers are of great interest due to their intriguing structural topologies [1–4]. Coordination polymers with various fascinating topologies have been extensively studied for their versatile chemical and physical properties and potential applications in functional materials [1,5–18].

Employing appropriate bridging ligands and choosing suitable metal ions are of great importance in the syntheses of coordination polymers. According to literature, polycarboxylate ligands have been shown to be good building blocks in the design of metal–organic materials with desired topologies due to their rich coordination modes. For instance, some complexes with pyridine-2,3-dicarboylate [19], pyrazine-2,3-dicarboxylic acid [20–30], pyrazine-2,3,5,6-tetracarboxylic acid, imidazole-4,5-dicarboxylic acid [31,32], and polybenzenecarboxylate ligand [33,34] have been reported.

We used pyrazine-2,3-dicarboxylic acid (H_2pzdc) in this work because H_2pzdc is a suitable multidentate bridging ligand to build polymeric coordination compounds [35]. Moreover, pyrazine-2,3-dicarboxylic acid was proved to be a versatile ligand and exhibited various coordination modes [20,36]. It often acts as chelating bidentate through one nitrogen atom and one oxygen atom of the adjacent carboxylate to form 1D or 2D structures similar to pyridine-2,3-dicarboxylic acid [37,38]. In addition, the solvent systems also play important roles in the formation of the molecular structure of the complexes [38–41]. To the best of our knowledge, studies on solvent-induced effects and the performance of the various ligands in modern coordination chemistry are very rare [42–44]. In order to investigate the influence of the solvent systems on the architecture of the supramolecular metal complexes, we have designed and synthesized two solvent-induced Cu(II) complexes by the complexation of pzdc with $Cu(CH_3COO)_2{\cdot}H_2O$, under the same exterior conditions in two different solvents in this work. Moreover, until now the six zinc complexes with pyrazine-2,3-dicarboxylate with different structure have been reported, $[Zn(pzdc)(H_2O)_2]{\cdot}H_2O$ [45], $\{[Zn(\mu\text{-}pzdc)(H_2O)_3]{\cdot}H_2O\}_n$ [46], $\{(H_3O)_2[Zn(\mu\text{-}pzdc)_2]\}_n$ [38], $[Zn_2(pzdc)_2(H_2O)_4]{\cdot}2.5H_2O$ [40], $[Zn(\mu\text{-}pzdc)(H_2O)_3]{\cdot}H_2O$ [40] and $\{[Zn(\mu\text{-}Hpzdc)(H_2O)_2]NO_3\}_n$ [41].

Our interest focuses on the Zn-based H_2pzdc for the self-assemblies of coordination polymers under different reaction conditions. In the present study we have reported two new 1D coordination polymers, which were constructed by the reaction of $ZnCl_2$, H_2pzdc and 2-meim. In fact, the main object of this study was to prepare a Zn(II)-pzdc complex with 2-meim ligand. However, $[Zn(\mu\text{-}pzdc)(H_2O)_3]_n$ (**4**) complex was obtained and 2-mim ligand was not coordinated to the Zn(II) ion. Again, we tried to synthesize the complex containing $ZnCl_2$, H_2pzdc and 2-meim at high pH by addition of the NH_3. Similar to **4**, 2-mim was not coordinated to Zn(II) ion and the formula of complex was determined as a

* Corresponding author. Tel.: +90 2222393750; fax: +90 2222393578.
E-mail address: yesilel@ogu.edu.tr (O.Z. Yeşilel).

0020-1693/$ - see front matter © 2012 Elsevier B.V. All rights reserved.
http://dx.doi.org/10.1016/j.ica.2012.12.036

$\{[Zn(\mu\text{-pzdc})(NH_3)_2(H_2O)]\cdot H_2O\}_n$ (**5**). The complexes **4** and **5** have different chain structure in contrast to the structures reported [38–41,45]. For example, $[Zn_2(pzdc)_2(H_2O)_4]\cdot 2.5H_2O$ and $[Zn(\mu\text{-pzdc})(H_2O)_3]\cdot H_2O$ complexes have been synthesized under hydrothermal condition at 150 °C for 72 h and 100 °C for 78 h, respectively [40]. These complexes display 1D square-wave-like chain and 1D ladder-like infinite chain structure, respectively. Similarly, $\{(H_3O)_2[Zn(\mu\text{-pzdc})_2]\}$ and $([Zn(pzdc)(H_2O)_2]\cdot H_2O$ are ribbon infinite chain structures and these complexes have been synthesized through facile synthesis.

Furthermore, imidazole, 1-methylimidazole and 2-methylimidazole have been considered as secondary ligands since these compounds are interesting. The imidazole ring is common in biologically important molecules. Thus, coordination complexes containing imidazole are appropriate models to study different aspects of biological molecules [47,48].

Recently, we reported the crystal structure, spectroscopic and thermal analyses of $\{[Cd(pzdc)(4\text{-mim})(5\text{-mim})_2]\cdot \tfrac{1}{2}H_2O\}_n$ [49], *mer*-$[Co(HOr)(H_2O)_2(2\text{-meim})_2]$ [50], $[Co(pzdca)(phen)_2]_2\cdot 11H_2O$ [51], *mer*-$[Mn(\mu\text{-HOr})(H_2O)(2\text{-meim})_2]_n$ [52], $\{[Co(\mu_{1,3}\text{-sq})(H_2O)_2(2\text{-Meim})_2]\cdot 2(2\text{-Meim})\}_n$ [53], $[Zn(4\text{-Meim})_2(5\text{-Meim})_2]sq\cdot 3H_2O$ [54], $[Cu_2(\mu\text{-pzdc})_2(pen)_2]\cdot 2H_2O$ [55], $[Cu(pydc)(H_2O)(4\text{-Meim})_2]\cdot H_2O$ [56], *trans*-$[Cu(H_2O)_2(4\text{-meim})_4](tdc)\cdot 4H_2O$ [57]. As a part of our current research on the syntheses and characterizations of mixed-ligand metal complexes of pzdc with N-donor ligands, in our present work we reported polynuclear and mononuclear Co(II), Cu(II), Zn(II) and Cd(II)–pyrazine-2,3-dicarboxylate (pzdc) complexes with im, 2-meim and NH_3 ligands: $[Co(\mu\text{-pzdc})(H_2O)(2\text{-meim})_2]_n$ (**1**), $[Cu(pzdc)(2\text{-meim})_3]\cdot DMF$ (**2**), $\{[Cu(\mu_3\text{-pzdc})(2\text{-meim})_2Cu(\mu\text{-pzdc})(2\text{-meim})]\cdot CH_3OH\cdot 2H_2O\}_n$ (**3**), $[Zn(\mu\text{-pzdc})(H_2O)_3]_n$ (**4**), $\{[Zn(\mu\text{-pzdc})(NH_3)_2(H_2O)]\cdot H_2O\}_n$ (**5**), $\{[Cd(\mu\text{-pzdc})(im)_3]\cdot 0.13H_2O\}_n$ (**6**), $\{[Cd(\mu\text{-pzdc})(N\text{-mim})_3]\cdot 3H_2O\}_n$ (**7**) and $[Cd(\mu\text{-pzdc})(2\text{-meim})_3]_n$ (**8**).

2. Experimental

2.1. Materials and measurements

All chemicals and solvents were purchased from commercial sources and were used without further purification. Elemental analyses for C, H and N were carried by a Elementar Vario El III. IR spectra of the complexes were determined as KBr discs using Bruker Tensor 27 FT-IR spectrometer within the 4000–400 cm^{-1} frequency range, magnetic susceptibility measurements were performed using a Sherwood Scientific MXI model Gouy magnetic balance at room temperature. The UV–Vis. spectrum was obtained for the DMF solution of the complex **2** (10^{-3} M) with a Shimadzu UV-3150 spectrometer in the range of 900–190 nm. The photoluminescence spectra for the solid complex sample was determined with a Perkin-Elmer LS-55 spectrometer. Thermal analyses were performed with a Diamond TG/DTA thermal analyser in static air atmosphere from 30 to 700 °C at a heating rate of 10 °C/min using platinum crucibles.

2.2. Crystallographic analyses

Diffraction experiments were carried out at 296 K on a Stoe IPDS diffractometer. The structure was solved by direct methods and refined using the programs SHELXS97 [58] and SHELXL97 [58]. All non-hydrogen atoms were refined anisotropically by full-matrix least-squares methods. The hydrogen atoms were placed in geometrically idealised positions and refined as riding atoms. Data collection: X-Area, cell refinement: X-Area, data reduction: X-RED, molecular graphics: Mercury program [59] were used. Details of data collection and crystal structure determinations are given in Table 1. The selected bond lengths, angles and hydrogen bonding geometry are given in Tables 2 and 3.

2.3. Details of molecular simulations

We performed atomically detailed simulations to make predictions about the gas storage capacities of materials synthesized in this work. Grand Canonical Monte Carlo (GCMC) simulations were used to compute adsorption of H_2 in all structures. Rigid and solvent-free structures were used in all molecular simulations. The universal force field (UFF) [60] was used for the framework atoms. A number of computational studies in the past showed that several general-purpose force fields including UFF employed in adsorption simulations of nanoporous materials give reasonable agreement with the measurements of experiments [61]. Spherical Lennard–Jones (LJ) 12–6 potentials were used to model H_2 (ε/k = 34.2 K, σ = 2.96 Å) [62]. These potential models have been successfully adopted in the past to predict adsorption behavior of gases in various nanoporous materials [63,64]. Interactions between adsorbate (H_2) and the atoms of pyrazine-2,3-dicarboxylate complexes were modeled using pair-wise interactions between adsorbates and each atom in the frameworks.

Mixed-atom interactions were defined using the Lorenz-Berthelot mixing rules. The interaction potential parameters used in the GCMC simulations are given in Table 4. Parameters ε and σ represent the energy and size parameters of the LJ potential (U_{LJ}), whereas r is the distance between particles:

$$U_{LJ} = 4\varepsilon_{ij}\left[\left(\frac{\sigma_{ij}}{r_{ij}}\right)^{12} - \left(\frac{\sigma_{ij}}{r_{ij}}\right)^{6}\right]$$

Conventional GCMC simulations were employed to compute single component adsorption isotherms of H_2 at 298 K. By specifying the temperature and fugacity of the adsorbing gases, the number of adsorbed molecules was calculated at equilibrium. The temperature was kept constant at 298 K in all GCMC simulations. Details of GCMC simulations can be found elsewhere [65]. For adsorption of single gas components, four types of trial moves, attempts to translate a molecule, attempts to rotate a molecule, attempts to create a new molecule, and attempts to delete an existing molecule were included. A cut-off distance of 13 Å was used for LJ interactions. The interactions of the adsorbates with the structures were pre-tabulated on a 0.2 Å grid. During the simulations, a 3D cubic Hermite polynomial interpolation scheme was used to calculate the potential at each point in space [66]. Periodic boundary conditions were applied in all simulations. The size of the simulation box was set to $2 \times 2 \times 2$ crystallographic unit cells. Simulations at the lowest fugacity for each system were started from an empty matrix and each subsequent simulation at higher fugacity was started from the final configuration of the previous run. Simulations included minimum 1×10^7 cycle equilibration period followed by a 1×10^7 cycle production run.

2.4. Antimicrobial activity tests

The antibacterial and antifungal properties of eight new complexes were investigated. In vitro antimicrobial activities of the synthesized new metal complexes were examined against two gram (−) bacteria (*Escherichia coli* ATCC25922, *Pseudomonas aeruginosa* ATCC27853), two gram (+) bacteria (*Bacillus cereus* ATCC7064, *Staphylococcus aureus* ATCC6535) and a yeast (*Candida albicans* ATCC10231). The results were compared to pyrazine-2,3-dicarbocxylic acid. The two (**2** and **7**) of new eight complexes solved in pure water, but six complexes did not dissolve in solvents (distilled water, ethanol, methanol and DMSO). Antimicrobial activity tests were carried out using the broth dilution method

Table 1
Crystal data and structure refinement parameters for complexes.

	1	2	3	4	5	6	7	8
Empirical formula	$C_{14}H_{16}CoN_6O_5$	$C_{21}H_{27}CuN_9O_5$	$C_{25}H_{30}Cu_2N_{10}O_{11}$	$C_6H_8N_2O_7Zn$	$C_6H_{10}N_4O_5Zn$	$C_{15}H_{14.25}CdN_8O_{4.13}$	$C_{18}H_{26}CdN_8O_7$	$C_{18}H_{20}CdN_8O_4$
Formula weight	407.26	549.06	773.67	285.51	283.55	484.99	578.87	524.82
Temperature (K)	293 (2)							
Wavelength (Å)	0.71073 Mo Kα							
Crystal system	orthorhombic	orthorhombic	triclinic	monoclinic	monoclinic	monoclinic	monoclinic	monoclinic
Space group	*Pbca*	$P2_12_12_1$	$P\bar{1}$	$P2_1/c$	$P2_1/c$	$C2/c$	$P2_1/c$	$P2_1$
a (Å)	13.817 (1)	7.2211 (3)	10.4454 (4)	5.4487 (7)	6.5661 (4)	20.450 (3)	9.4194 (3)	8.633 (1)
b (Å)	15.312 (2)	15.0796 (6)	11.6829 (4)	15.404 (2)	21.5954 (13)	9.784 (1)	24.4525 (12)	12.576 (1)
c (Å)	16.024 (1)	23.6400 (9)	15.9242 (6)	11.931 (1)	7.8310 (4)	18.850 (2)	10.5548 (4)	9.864 (1)
α (°)	90	90	69.168 (3)	90	90	90	90	90
β (°)	90	90	72.880 (2)	114.76 (1)	115.854 (4)	100.595 (9)	96.445 (3)	94.866 (6)
γ (°)	90	90	74.300 (3)	90	90	90	90	90
V (Å^3)	3390.1 (5)	2574.2 (2)	1705.6 (1)	909.4 (2)	999.3 (1)	3707.2 (6)	2415.7 (2)	1067.1 (1)
Z	8	4	2	4	4	8	4	2
Absorption coefficient (mm^{-1})	1.05	0.90	1.32	2.73	2.47	1.22	0.96	1.07
D_{calc} (Mg m^{-3})	1.596	1.417	1.507	2.085	1.885	1.738	1.592	1.633
Theta range for data collection (°)	1.5–28.0	1.4–27.2	1.9–27.2	1.9–28.2	1.9–27.3	2.03–26.50	1.7–27.3	2.1–28.0
Measured reflections	18002	20687	32962	5727	6175	39815	15096	6232
Independent reflections	3518	5313	7122	1885	2101	3851	5002	4678
Absorption correction	Integration Stoe X–RED (Stoe and Cie, 2001)							
Refinement method	Full–matrix least–squares on F^2							
Final *R* indices [$I > 2\sigma(I)$]	R_{int} = 0.028	R_{int} = 0.102	R_{int} = 0.068	R_{int} = 0.132	R_{int} = 0.028	R_{int} = 0.062	R_{int} = 0.031	R_{int} = 0.024
Final *R* indices (all data)	R1 = 0.030 wR2 = 0.081	R1 = 0.071 wR2 = 0.189	R1 = 0.058 wR2 = 0.173	R1 = 0.052 wR2 = 0.083	R1 = 0.025 wR2 = 0.068	R1 = 0.027 wR2 = 0.070	R1 = 0.024 wR2 = 0.064	R1 = 0.025 wR2 = 0.066
Goodness-of-fit on F^2	1.05	1.01	1.12	1.11	1.10	1.05	1.06	1.05
$\Delta\rho_{max}$ (e Å^{-3})	0.27	0.48	0.78	0.95	0.29	0.36	0.35	0.27
$\Delta\rho_{min}$ (e Å^{-3})	−0.35	−0.52	−1.43	−0.97	−0.39	−1.04	−0.43	−0.85

(NCCLS 2007 procedure). The cultures were grown in 5 mL nutrient broth (Merck) at 37 °C for 18 h at 175 rpm in an orbital shaker incubator. Initial bacterial concentrations (approximately 5×10^5 cfu/mL) were estimated for the cultures by matching with 0.5 McFarland standards at 600 nm. New complexes were tested in twofold serial dilution; eventually the ranges were narrowed to define more exact values. Minimal inhibitory concentration (MIC) value was determined as the lowest concentration at which the growth of microorganisms was not observed.

2.5. Synthesis of the complexes

2.5.1. $[Co(\mu\text{-pzdc})(H_2O)(2\text{-meim})_2]_n$ (**1**)

A solution of H_2pzdc (0.50 g, 3 mmol) in water (25 mL) was added dropwise with stirring at 50 °C to a solution of $CoCl_2{\cdot}6H_2O$ (0.54 g, 3 mmol) in distilled water (25 mL). The solution abruptly became suspension and was stirred for 4 h at 50 °C. Then the 2-meim ligand (0.40 g, 6 mmol) in water (10 mL) was added dropwise to this suspension. The clear solution was stirred for 3 h at 50 °C and then cooled to room temperature. The single crystals of **1** were formed, filtered, washed with 10 mL of water and dried in air. *Anal.* Calc. for $C_{14}H_{16}CoN_6O_5$: C, 37.37; H, 2.35; N, 14.53. Found: C, 37.33; H, 2.52; N, 14.26%; IR (cm^{-1}, KBr): ν(H_2O), 3286 s; ν(NH), 3114 m; ν(CH), 3069 w, 2974 w, 2750 w, 2634 w; ν_{as}(COO), 1649 vs 1595 vs; ν(C=N), 1489 m; ν_s(COO), 1388 s, 1348 s.

2.5.2. $[Cu(pzdc)(2\text{-meim})_3]{\cdot}DMF$ (**2**)

Ten milliliters of water solution of H_2pzdc (0.50 g, 3 mmol) was treated with 10 mL NH_3 (25%) under stirring at 50 °C. The solution was added $Cu(CH_3COO)_2{\cdot}H_2O$ (0.59 g, 3 mmol) and immediately precipitated. This suspension was stirred for 1 h at 50 °C. Then the 2-meim ligand (0.40 g, 6 mmol) in dimethylformamide/water mixtures (1:2; 15 mL) was added dropwise to this suspension. The clear solution was stirred for 2 h at 50 °C and then cooled to room temperature. The blue crystals of **2** were formed, filtered, washed with 10 mL of water and dried in air. *Anal.* Calc. for $C_{21}H_{27}CuN_9O_5$: C, 45.94; H, 4.96; N, 22.96. Found: C, 46.01; H, 4.77; N, 23.10%; IR (cm^{-1}, KBr): ν(NH), 3118 m; ν(CH), 3118 m, 3080 m, 2962 m, 2790 m, 2698 m; ν_{as}(COO), 1643 vs 1593 vs; ν(C=N), 1490 m; ν_s(COO), 1375 s, 1348 s.

2.5.3. $\{[Cu(\mu_3\text{-pzdc})(2\text{-meim})_2Cu(\mu\text{-pzdc})(2mim)]{\cdot}CH_3OH{\cdot}2H_2O\}_n$ (**3**)

The preparation method is similar to that of complex **2** and methanol was used instead of dimethylformamide. *Anal.* Calc. for $C_{25}H_{30}Cu_2N_{10}O_{11}$: C, 38.81; H, 18.10; N, 3.91. Found: C, 38.79; H, 18.14; N, 3.87%; IR (cm^{-1}, KBr): ν(H_2O), 3421 s; ν(NH), 3209 s, ν(CH), 3124 w, 2927 w; ν_{as}(COO), 1658 vs 1608 vs 1575 s; ν(C=N), 1492 m; ν_s(COO), 1386 s, 1350 s.

2.5.4. $[Zn(\mu\text{-pzdc})(H_2O)_3]_n$ (**4**) and $\{[Zn(\mu\text{-pzdc})(NH_3)_2(H_2O)]{\cdot}H_2O\}_n$ (**5**)

In the complex **4**, the solution of H_2pzdc (0.50 g, 3 mmol) in water (25 mL) was added dropwise with stirring at 50 °C to a solution of $ZnCl_2$ (0.41 g, 3 mmol) in distilled water (15 mL). The solution abruptly became suspension and precipitated. Then the 2-meim ligand (0.40 g, 6 mmol) in water (5 mL) was added dropwise to this suspension. The suspension was stirred for 5 h at 70 °C. After filtering, it was put aside for crystallization process. In a few days the crystals of complex **4** were obtained.

The preparation method of complex **5** is similar to that of complex **4,** however in complex **5;** when the precipitate was occurred, NH_3 was added, solution formation was observed and then cooled to room temperature. The single crystals of **4** and **5** were filtered and washed with 10 mL of water and dried in air. In fact, the aim of this study was to synthesize a Zn(II)-pzdc complex with 2-meim ligand. However, 2-meim ligand does not coordinate Zn(II) ion in the complexes **4** and **5** and surprisingly, two new complexes of Zn(II)-pzdc with aqua and amine ligands were obtained.

Table 2
The bond distances and angles in the complexes (Å, °).

*Complex **1***			
Co1–N1	2.158 (2)	Co1–O1	2.088 (1)
Co1–N3	2.132 (2)	Co1–O5	2.162 (1)
Co1–N5	2.118 (2)	Co1^{i}–O4	2.112 (1)
O1–Co1–O4^{ii}	166.90 (5)	N5–Co1–N1	170.81 (6)
O1–Co1–N5	95.06 (6)	N3–Co1–N1	85.97 (6)
O4^{ii}–Co1–N5	96.94 (6)	O1–Co1–O5	88.42 (5)
O1–Co1–N3	95.99 (6)	O4^{ii}–Co1–O5	85.69 (5)
O4^{ii}–Co1–N3	89.02 (6)	N5–Co1–O5	93.13 (6)
N5–Co1–N3	91.19 (6)	N3–Co1–O5	173.54 (6)
O1–Co1–N1	76.58 (5)	N1–Co1–O5	90.47 (6)
O4^{ii}–Co1–N1	91.76 (5)		
*Complex **2***			
N1–Cu1	2.050 (5)	N7–Cu1	2.028 (6)
N3–Cu1	2.027 (7)	O1–Cu1	2.168 (4)
N5–Cu1	1.976 (6)		
N5–Cu1–N3	91.4 (3)	N7–Cu1–N1	88.5 (3)
N5–Cu1–N7	90.5 (3)	N5–Cu1–O1	97.5 (2)
N3–Cu1–N7	154.7 (2)	N3–Cu1–O1	105.7 (3)
N5–Cu1–N1	175.6 (2)	N7–Cu1–O1	99.1 (3)
N3–Cu1–N1	91.3 (3)	N1–Cu1–O1	78.44 (18)
*Complex **3***			
N1–Cu1	2.035 (4)	N7–Cu2	2.021 (3)
N3–Cu1	1.994 (4)	N9–Cu2	1.971 (3)
N5–Cu1	1.978 (4)	O4–Cu2	1.960 (3)
O1–Cu1	1.961 (3)	O5–Cu2	1.962 (3)
O3–Cu1	2.281 (3)	O7–Cu2	2.220 (3)
O1–Cu1–N5	92.18 (16)	O4–Cu2–O5	171.08 (13)
O1–Cu1–N3	159.31 (17)	O4–Cu2–N9	94.34 (13)
N5–Cu1–N3	92.35 (17)	O5–Cu2–N9	88.96 (13)
O1–Cu1–N1	80.80 (13)	O4–Cu2–N7	93.24 (12)
N5–Cu1–N1	170.25 (16)	O5–Cu2–N7	81.40 (12)
N3–Cu1–N1	91.95 (15)	N9–Cu2–N7	162.48 (15)
O1–Cu1–O3	98.54 (14)	O4–Cu2–O7	86.05 (11)
N5–Cu1–O3	99.41 (16)	O5–Cu2–O7	101.36 (13)
N3–Cu1–O3	100.62 (14)	N9–Cu2–O7	102.25 (14)
N1–Cu1–O3	88.38 (13)	N7–Cu2–O7	94.01 (13)
*Complex **4***			
N1–Zn1^{i}	2.145 (2)	O1–Zn1	2.037 (2)
O4–Zn1^{i}	2. 071 (2)	O5–Zn1	2.162 (2)
O6–Zn1	2.015 (2)	O7–Zn1	2.380 (3)
O6–Zn1–O1	97.48 (10)	O4^{ii}–Zn1–O5	100.87 (8)
O6–Zn1–O4^{ii}	166.90 (10)	N2^{ii}–Zn1–O5	89.89 (8)
O1–Zn1–O4^{ii}	87.93 (8)	O6–Zn1–O7	79.69 (9)
O6–Zn1–N2^{ii}	98.07 (10)	O1–Zn1–O7	108.89 (9)
O1–Zn1–N2^{ii}	162.91 (9)	O4^{ii}–Zn1–O7	87.27 (8)
O4^{ii}–Zn1–N2^{ii}	78.40 (8)	N2^{ii}–Zn1–O7	80.93 (9)
O6–Zn1–O5	91.68 (9)	O5–Zn1–O7	166.31 (8)
O1–Zn1–O5	82.60 (8)		
*Complex **5***			
N1–Zn1	2.1892 (16)	O1–Zn1	2.1120 (14)
N3–Zn1	2.1011 (19)	O4–Zn1^{i}	2.0877 (14)
N4–Zn1	2.0541 (18)	Zn1–O5	2.3365 (18)
N4–Zn1–O4^{ii}	95.57 (6)	N3–Zn1–N1	88.85 (7)
N4–Zn1–N3	99.36 (8)	O1–Zn1–N1	76.12 (6)
O4^{ii}–Zn1–N3	89.62 (7)	N4–Zn1–O5	90.82 (7)
N4–Zn1–O1	89.67 (6)	O4^{ii}–Zn1–O5	86.91 (6)
O4^{ii}–Zn1–O1	169.35 (6)	N3–Zn1–O5	169.52 (7)
N3–Zn1–O1	98.70 (7)	O1–Zn1–O5	83.74 (6)
N4–Zn1–N1	164.58 (7)	N1–Zn1–O5	81.81 (6)
O4^{ii}–Zn1–N1	97.53 (6)		
*Complex **6***			
N1–Cd1	2.408 (2)	N7–Cd1	2.327 (2)
N3–Cd1	2.356 (2)	O1–Cd1	2.389 (2)
N5–Cd1	2.290 (2)	O2–Cd1^{i}	2.352 (2)
N5–Cd1–N7	99.65 (8)	O2^{ii}–Cd1–O1	165.34 (6)
N5–Cd1–O2^{ii}	83.27 (6)	N3–Cd1–O1	101.59 (7)
N7–Cd1–O2^{ii}	88.18 (7)	N5–Cd1–N1	149.55 (7)
N5–Cd1–N3	85.19 (8)	N7–Cd1–N1	95.98 (8)
N7–Cd1–N3	174.11 (8)	O2^{ii}–Cd1–N1	123.38 (6)
O2^{ii}–Cd1–N3	89.08 (7)	N3–Cd1–N1	81.21 (7)
N5–Cd1–O1	87.60 (6)	O1–Cd1–N1	68.83 (6)
N7–Cd1–O1	82.05 (6)		
*Complex **7***			
N1–Cd1	2.4150 (15)	N7–Cd1	2.3028 (16)
N3–Cd1	2.3477 (17)	O1–Cd1	2.3530 (14)
N5–Cd1	2.2932 (16)	O2–Cd1^{i}	2.2907 (14)
O2^{ii}–Cd1–N5	90.55 (6)	N7–Cd1–O1	94.47 (6)
O2^{ii}–Cd1–N7	99.23 (6)	N3–Cd1–O1	84.47 (6)
N5–Cd1–N7	88.99 (6)	O2^{ii}–Cd1–N1	114.44 (5)
O2^{ii}–Cd1–N3	81.91 (6)	N5–Cd1–N1	154.94 (6)
N5–Cd1–N3	92.80 (7)	N7–Cd1–N1	85.38 (6)
N7–Cd1–N3	177.88 (6)	N3–Cd1–N1	92.52 (6)
O2^{ii}–Cd1–O1	166.11 (5)	O1–Cd1–N1	68.78 (5)
N5–Cd1–O1	87.39 (6)		
*Complex **8***			
N1–Cd1	2.426 (2)	N7–Cd1	2.317 (3)
N3–Cd1	2.351 (2)	O1–Cd1	2.395 (2)
N5–Cd1	2.288 (2)	Cd1–O3^{i}	2.265 (2)
O3^{i}–Cd1–N5	104.51 (10)	N7–Cd1–O1	87.65 (9)
O3^{i}–Cd1–N7	90.91 (9)	N3–Cd1–O1	86.27 (9)
N5–Cd1–N7	100.11 (9)	O3^{i}–Cd1–N1	82.16 (7)
O3^{i}–Cd1–N3	91.73 (9)	N5–Cd1–N1	170.50 (8)
N5–Cd1–N3	86.78 (9)	N7–Cd1–N1	86.37 (9)
N7–Cd1–N3	171.76 (10)	N3–Cd1–N1	86.26 (9)
O3^{i}–Cd1–O1	151.24 (7)	O1–Cd1–N1	69.07 (7)
N5–Cd1–O1	104.01 (9)		

Symmetry codes: (i) $x-½, -y+½, -z+2$; (ii) $x+½, -y+½, -z+2$ for **1**; (i) $x-1, y, z-1$; (ii) $x+1, y, z+1$ for **4**; (i) $-x+½, y-½, -z+½$; (ii) $-x+½, y+½, -z+½$ for **5**; (i) $x, -y+½, z+½$; (ii) $x, -y+½, z-½$ for **6** and (i) $-x+1, y+½, -z+1$ for **7**; (i) $1-x+½+y, 1-z$ for **8**.

Anal. Calc. for $C_6H_8N_2O_7Zn$ (**4**): C, 25.24; H, 9.81; N, 2.82. Found: C, 25.21; H, 9.53; N, 2.79%; IR (cm^{-1}, KBr): $\nu(H_2O)$, 3457 vs; 3251 vs; ν_{as}(COO), 1643 vs 1573 vs; ν(C=N), 1469 m; ν_s(COO), 1361 vs.

Anal. Calc. for $C_6H_{10}N_4O_5Zn$ (**5**): C, 25.41; H, 3.55; N, 19.76. Found: C, 25.18; H, 3.43; N, 19.58%; IR (cm^{-1}, KBr): $\nu(H_2O)$, 3363 vs; $\nu(NH_3)$, 3334 vs; $\nu(NH_3)$, 3275 s, 3246 w, 3194 w; ν_{as}(COO), 1652 vs 1593 vs; ν(C=N), 1433 m; ν_s(COO), 1394 vs 1361 vs.

2.5.5. $\{[Cd(\mu\text{-pzdc})(im)_3]\cdot 0.13H_2O\}_n$ (**6**)

A solution of pyrazine-2,3-dicarboxylic acid (0.50 g, 3 mmol) in water (25 mL) was added dropwise with stirring at 50 °C to a solution of $CdCl_2\cdot H_2O$ (0.54 g, 3 mmol) in distilled water (25 mL). The solution immediately became suspension and was stirred for 1 h at 50 °C. Then the imidazole ligand (0.40 g, 6 mmol) in water (10 mL) was added dropwise to this suspension. The clear solution was stirred for 3 h at 50 °C and then cooled to room temperature. The single crystals of **6** were filtered and washed with 10 mL of water and dried in air. *Anal.* Calc. for $C_{15}H_{14.25}CdN_8O_{4.13}$: C, 37.14; H, 2.96; N, 23.10. Found: C, 36.43; H, 2.77; N, 22.99%; IR (cm^{-1}, KBr): $\nu(H_2O)$, 3408 s; ν(NH), 3132 s; ν(CH), 3053 s, 2949 m, 2864 m, 2721 m; ν_{as}(COO), 1616 vs 1562 vs; ν(C=N), 1537 m; ν_s(COO), 1394 vs 1359.

2.5.6. $\{[Cd(\mu\text{-pzdc})(N\text{-mim})_3]\cdot 3H_2O\}_n$ (**7**) and $[Cd(\mu\text{-pzdc})(2\text{-meim})_3]$ (**8**)

The preparation methods of complexes **7** and **8** are similar to that of complex **6** and N-mim and 2-meim ligands were used instead of imidazole, respectively.

Anal. Calc. for $C_{18}H_{26}N_8O_7Cd$ (**7**): C, 37.35; H, 19.36; N, 4.53. Found: C, 37.38; H, 19.42; N, 4.56%; IR (cm^{-1}, KBr) for **7**: $\nu(H_2O)$, 3400 vs; ν(NH), 3114 s; ν(CH), 3069 w, 2974 w, 2750 w, 2634 w; ν_{as}(COO), 1620 vs 1585 vs; ν(C=N), 1431 s; ν_s(COO), 1386 s, 1355vs.

Calc. for $C_{18}H_{20}N_8O_4Cd$ (**8**): C, 41.19; H, 3.84; N, 21.35. Found: C, 41.73; H, 3.69; N, 21.16%: IR (cm^{-1}, KBr) for **8**: $\nu(H_2O)$, 3239 s; ν(NH), 3135 s; ν(CH), 3057 m, 2957 m, 2918 m, 2856 m; ν_{as}(COO), 1640 vs 1594 vs; ν(C=N), 1492 m; ν_s(COO), 1385 s, 1355 s; $\Delta\nu$, 255, 239.

Table 3
Hydrogen bonding interactions in the complexes.

D–H···*A*	*D*–H	H···*A*	*D*···*A*	*D*–H···*A*
Complex ***1***				
N4–H4···O2^{iii}	0.86	2.17	2.902 (2)	143
N4–H4···O3^{iii}	0.86	2.39	3.009 (2)	129
N6–H6···O3^{iv}	0.86	2.16	2.944 (2)	151
O5–H5A···O3^{ii}	0.84 (2)	1.94 (2)	2.743 (2)	158 (2)
O5–H5B···O1^{v}	0.80 (2)	1.97 (2)	2.774 (2)	177 (3)
Complex ***2***				
N4–H4···O4^{i}	0.86	1.86	2.702 (10)	167
N6–H6···O5^{ii}	0.86	2.32	3.036 (18)	141
N8–H8A···O3^{iii}	0.86	1.92	2.761 (10)	167
C1–H1···O2^{iv}	0.93	2.27	3.154 (8)	159
Complex ***3***				
N4–H4···O8^{iii}	0.86	2.07	2.914 (5)	167
N4–H4···O7^{iii}	0.86	2.42	3.065 (5)	132
N6–H6···O11^{iv}	0.86	2.11	2.959 (7)	170
N10–H10···N8^{v}	0.86	2.12	2.970 (5)	171
O11–H11B···O6^{vi}	0.82 (5)	2.31 (5)	2.993 (6)	140 (7)
O11–H11B···O8^{vii}	0.82 (5)	2.54 (7)	3.085 (6)	125 (7)
O11–H11A···O8	0.83 (6)	2.03 (4)	2.807 (5)	156 (7)
O12–H12B···O13	0.89 (7)	2.23 (7)	3.093 (11)	163 (4)
C25–H25A···O2^{i}	0.96	2.16	2.920 (15)	135
Complex ***4***				
O5–H5A···N1^{iii}	0.81 (2)	2.17 (2)	2.969 (3)	172 (4)
O5–H5B···O4^{iv}	0.82 (2)	2.01 (2)	2.815 (3)	169 (4)
O6–H6A···O2^{iii}	0.82 (2)	1.84 (2)	2.660 (3)	176 (5)
O6–H6B···O3^{v}	0.81 (2)	2.13 (2)	2.892 (3)	155 (5)
O6–H6B···O2^{v}	0.81 (2)	2.40 (4)	2.874 (3)	119 (4)
O7–H7A···O2	0.82 (2)	2.40 (5)	2.884 (3)	119 (5)
O7–H7A···O2^{vi}	0.82 (2)	2.38 (3)	3.166 (3)	163 (4)
O7–H7B···O3^{v}	0.82 (2)	2.06 (2)	2.842 (3)	159 (4)
Complex ***5***				
N3–H3A···O3^{iii}	0.89	2.25	3.118 (3)	164
N3–H3B···N2^{iv}	0.89	2.37	3.227 (3)	163
N3–H3C···O5^{iii}	0.89	2.34	3.185 (3)	158
N4–H4A···O2^{ii}	0.89	2.06	2.929 (2)	167
N4–H4B···O2^{v}	0.89	2.33	3.171 (3)	158
N4–H4C···O1^{vi}	0.89	2.13	3.020 (2)	174
O5–H7A···O3^{ii}	0.83 (2)	1.92 (2)	2.733 (2)	164 (3)
O5–H7B···O2^{v}	0.84 (2)	1.97 (2)	2.780 (2)	163 (3)
Complex ***6***				
N4–H4A···O3^{iii}	0.86	2.32	2.914 (3)	127
N4–H4A···N2^{iv}	0.86	2.45	3.080 (3)	131
N6–H6···O3^{v}	0.86	1.95	2.739 (3)	153
N8–H8A···O4^{vi}	0.86	1.89	2.721 (3)	163
O5–H5···O4^{iv}	0.83 (2)	1.93 (7)	2.727 (9)	161 (20)
Complex ***7***				
O5–H5A···O6	0.84 (1)	2.12 (2)	2.945 (3)	170 (4)
O5–H5B···O3^{iii}	0.85 (1)	2.09 (1)	2.933 (3)	171 (4)
O6–H6A···O3^{iv}	0.86 (2)	2.05 (2)	2.861 (3)	158 (4)
O6–H6A···O4^{iv}	0.86 (2)	2.54 (3)	3.265 (3)	143 (3)
O6–H6B···O4	0.85 (2)	1.92 (2)	2.757 (3)	169 (4)
O7–H7A···O6	0.86 (2)	2.03 (2)	2.884 (4)	169 (6)
Complex ***8***				
N4–H4···O4^{ii}	0.86	1.94	2.755 (4)	159
N6–H6···O2^{iii}	0.86	2.00	2.859 (3)	172
N8–H8A···O2^{iv}	0.86	2.04	2.848 (3)	157

Symmetry codes: (ii) $x+½, -y+½, -z+2$; (iii) $x+½, y, -z+3/2$; (iv) $-x+1, y-½, -z+3/2$; (v) $-x+1, -y, -z+2$ for **1**; (i) $x+1/2, -y+1/2, -z+1$; (ii) $-x+3/2, -y+1, z+1/2$; (iii) $x+1/2, -y+3/2, -z+1$; (iv) $x+1, y, z$; for **2**; (i) $-x+2, -y+1, -z$; (iii) $x-1, y, z$; (iv) $-x+2, -y+1, -z+1$; (v) $x, y+1, z$; (vi) $x+1, y, z$; (vii) $-x+3, -y, -z+1$ for **3**; (iii) $x-1, y, z$; (iv) $-x, y-1/2, -z+3/2$; (v) $-x, -y+1, -z+1$; (vi) $-x+1, -y+1, -z+1$ for **4**; (ii) $x+1, y, z+1$; (iii) $x+1, y, z$; (iv) $x+1, -y+3/2, z+1/2$; (v) $-x+1, -y+2, -z+1$; (vi) $-x+2, -y+2, -z+1$ for **5**; (iii) $x, -y+1, z-½$; (iv) $-x+1, y, -z+½$; (v) $x-½, -y+½, z-½$; (vi) $x-½, y+½, z$ for **6**; (iii) $x-1, y, z$; (iv) $-x+1, -y, -z+1$ for **7** and (ii) $-x, y+½, -z+1$; (iii) $-x+1, y+½, -z+2$; (iv) $x+1, y, z$ for **8**.

2.6. UV–Vis spectra and magnetic susceptibilities

The electronic spectrum of **2** in DMF shows intense bands between 250 and 278 are assigned to the $\pi \rightarrow \pi^*$ and $n \rightarrow \pi^*$ transitions of the 2-meim and DMF molecules, respectively. The UV–Vis spectrum of the complex **2** exhibits very broad d–d absorption bands at 671 nm ($\varepsilon = 36.2$ Lmol^{-1} cm^{-1}). This value was assigned to the $a_1 \rightarrow b_1$ and $b_2 \rightarrow b_1$ transitions for **2**, thereby suggesting square pyramidal geometry around Cu(II) for **2**. The other complexes (common solvents, which are not able to dissolve the coordination polymers (**1** and **3**–**8**)) failed to provide spectra.

Complex **1** exhibits the magnetic moment value of 4.06 BM, which corresponds to three of the unpaired electrons. These values are higher than the spin-only value of 3.87 BM. This is not only due to the spin magnetic moment that contributes to the total magnetic moment but also due to the orbital magnetic moment in Co(II) complexes. Magnetic moment values of **2** and **3** were measured as 1.71 and 1.25 BM, respectively, which correspond to one unpaired electron. The Zn(II) and Cd(II) complexes are diamagnetic.

Table 4
Interaction potential parameters for adsorbent atoms used in this work.

Atoms/molecules	ε/k_B (K)	σ (Å)
C	52.87	3.43
Cd	114.81	2.54
Co	7.05	2.56
Cu	2.52	3.11
H	22.16	2.57
N	34.75	3.26
O	30.21	3.12
Zn	62.44	2.46

3. Crystal structures

3.1. $[Co(\mu\text{-pzdc})(H_2O)(2\text{-meim})_2]_n$ (*1*)

The crystal structure of **1** with the atom labeling is shown in Fig. 1. The selected bond lengths, angles and hydrogen bonding geometry are given in Tables 2 and 3. The complex crystallizes in the orthorhombic space group *Pbca*. The Co(II) ion is coordinated by the two pzdc, two 2-meim and one aqua ligands forming distorted octahedral geometry. The pzdc ligand acts as tridentate bridging ligand through deprotonated oxygen atom of carboxylate group and nitrogen atom of pyridine ring as a chelate manner and oxygen atom of other carboxyl group (Scheme 1a). The Co1–O1 (2.088 (1) Å) and Co1–N1 (2.158 (2) Å) bond distances are similar to the ones found in the $[Co(pzdc)(phen)_2]_2{\cdot}11H_2O$, $(H_2tmen)[Co(pzdca)_2(tmen)]{\cdot}9H_2O$ [51], $[Co_2(pzdc)_2(bipy)(H_2O)_2]_n{\cdot}3nH_2O$, $[Co(pydc)_2(H_2O)_2](H_2bipy)$ [67], and $\{[Co(phen)(\mu\text{-pzdc})]{\cdot}H_2O\}_n$ [29]. The carboxylate C–O distances in the pzdc anion also display

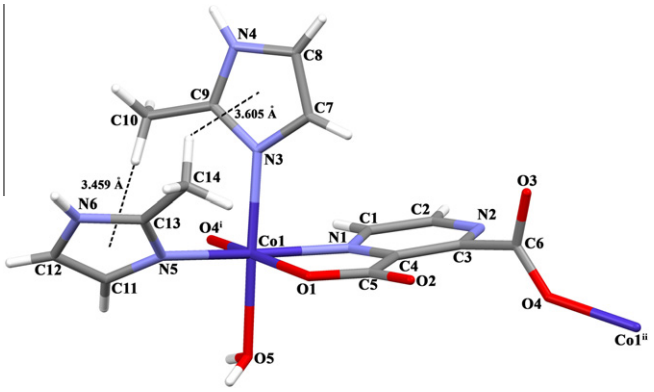

Fig. 1. Molecular structure of $[Co(\mu\text{-pzdc})(H_2O)(2\text{-meim})_2]_n$ (**1**) with atom-labeling scheme.

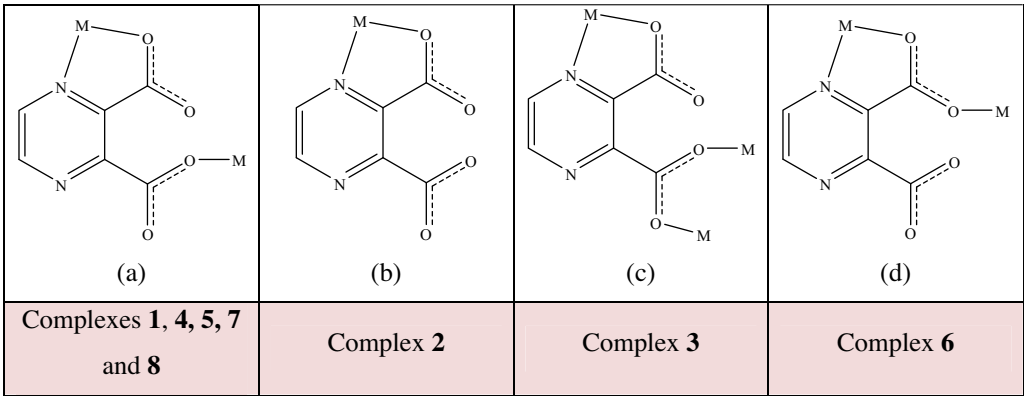

Scheme 1. Coordination modes for the pzdc ligand in **1**–**8**.

some variability depending on their environment [C5–O1 = 1.266 (2), C5–O2 = 1.232 (2), C6–O3 = 1.245 (2) and C6–O4 = 1.248 (2) Å]. The carboxylate group involved in chelation is almost coplanar with the pyridine ring and the other carboxylate group is twisted by 86.53 Å.

The crystal packing of complex is a composite of intermolecular hydrogen bonding and C–H···π interactions. The complex exhibits a number of intermolecular N–H···O and O–H···O hydrogen bonds as given in Table 3. It is seen from Fig. 2 that the hydrogen bonds between the aqua ligand and the coordinated carboxylate O atom of pzdc ligand constitute $R_2^2(8)$ rings [O5···O1 = 2.774 (2) and O5···O3 = 2.743(2) Å]. There are also the intermolecular N–H···O hydrogen bonding between the oxygen atom (O2 and O3) of the carboxylate group and nitrogen atom (N4 and N6) of 2-meim ligands [N4···O2 = 2.902 (2), N4···O3 = 3.009 (2), N6···O3 = 2.944 (2)] with a pattern $R_1^2(7)$. Furthermore, there are C–H···π interactions between imidazole rings [Cg1 = N3–C7–C8–N4–C9 and Cg2 = N5–C11–C12–N6–C13, H14B···Cg1 = 3.6047 Å, C14–H14B···Cg1 = 122°; C10–H10B···Cg3 = 3.4591 Å, C10–H10B···Cg3 = 138° and H12···Cg2^{i} = 3.4732 Å, C12–H12···Cg2^{i} = 144° (i = 1/2 − *x*, 1/2 + *y*, *z*) (Fig. 1). All of these intermolecular interactions give rise to a three dimensional network.

3.2. [Cu(pzdc)(2-meim)$_3$]·DMF (**2**)

The molecular structure with atomic numbering scheme of complex **2** is shown in Fig. 3. The X-ray structural analysis reveals that **2** crystallizes in the orthorhombic $P2_12_12_1$ space group. The Cu(II) ion is coordinated by one carboxyl oxygen (O1), one pyrazine nitrogen atoms (N1) from one pzdc ligand and three nitrogen atoms (N3, N5 and N7) of the three 2-meim ligands, having a distorted square pyramidal geometry (Scheme 1b). The four nitrogen atoms comprise the equatorial plane, while carboxyl oxygen atom occupying the axial position. The Cu1–O1 and Cu1–N1 bond distances being 2.168 (4) and 2.050 (5) Å, respectively. These values are similar to that in complex {[Cu(μ-pzdc)(H_2O)$_3$]·H_2O}$_n$ [68]. The complex **2** has a τ value of 0.348 [τ = 175.6–154.7)/60 = 0.348]. The τ values clearly indicate that the copper atom in **2** is distorted square pyramidal geometry [69].

The crystal packing analysis indicate that the crystal packing of **2** is formed via intermolecular hydrogen bonding and weak C–H···π interactions. The hydrogen bonding geometries are given in Table 3. Adjacent complex units are further extended to a 2D hydrogen-bonded layered network through the intermolecular N–H···O hydrogen bond between the N–H group of 2-meim ligand

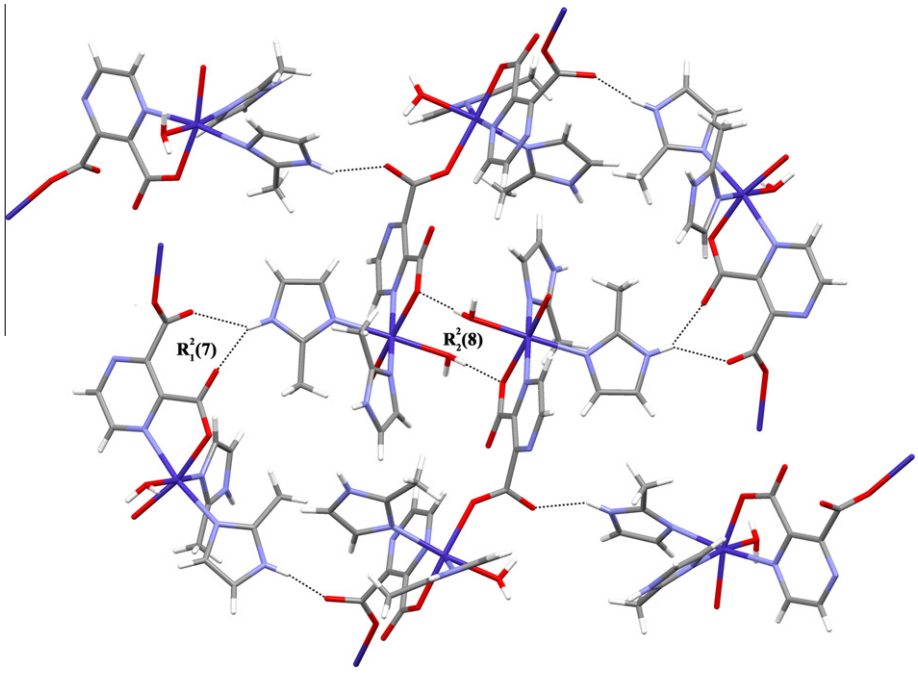

Fig. 2. Intermolecular hydrogen-bonding geometry and view of $R_1^2(7)$ ve $R_2^2(8)$ motifs of **1**.

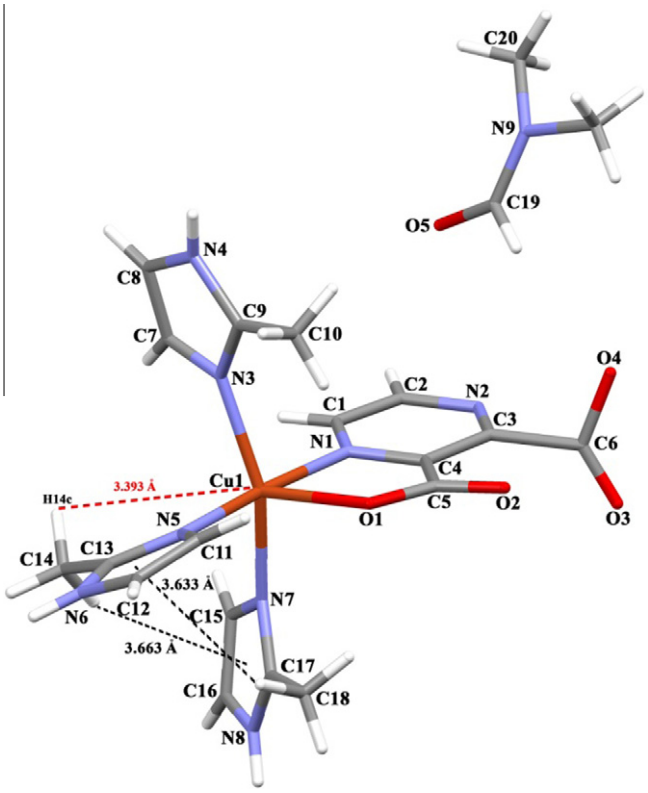

Fig. 3. Molecular structure of [Cu(pzdc)(2-meim)$_3$]·DMF (**2**) with atom-labeling scheme.

and carboxyl oxygen atoms of pzdc ligand. The two-dimensional layers stacked one another through the C–H···π interactions between the C21–H21B of DMF molecule and the imidazole ring (Cg1) [C21–H21B···Cg1 = 3.743 Å and 140°], giving rise to a three-dimensional supramolecular architecture (Fig. 4).

3.3. {[Cu(μ_3-pzdc)(2-meim)$_2$Cu(μ-pzdc)(2-meim)]·CH_3OH·$2H_2O$}$_n$ (**3**)

The molecular structure with atomic numbering scheme of **3** is shown in Fig. 5. The X-ray structural analysis reveals that **3** crystallizes in the triclinic, $P\bar{1}$ space group with the asymmetric unit that contains Cu(II) ions exhibiting two different coordination environments with two pzdc ligands, three 2-meim ligands, two lattice water and one methanol molecules. It is noted that when DMF was replaced by CH_3OH, a 1-D polymeric chain structure of **3** was formed instead of the previous mononuclear structure of **2**. As shown in Fig. 5, the Cu1 atom is coordinated by two carboxyl oxygen atoms (O1 and O3^i) and one nitrogen atom (N1) from two pzdc ligands and two nitrogen atoms (N3 and N5) from two 2-meim ligands, forming a distorted square-pyramidal geometry (Scheme 1c). The four atoms (O1, N1, N3 and N5) form the basal plane. The O3^i atom occupies the apical site. The Cu2 atom has a distorted square-pyramidal geometry with the basal plane defined by N7, N9, O4 and O5 atoms from the three pzdc and one 2-meim ligands. The carboxyl oxygen atom (O7^{ii}) occupies the apical position. The Cu–N and Cu–O bond distances in **3** are in the ranges of 1.971 (3)–2.035 (4) Å and of 1.960 (3)–2.281 (3) Å, respectively. It is similar to the corresponding one in the known copper complex [24,55,70,71], as shown in Table 2. The Cu1 and Cu2 have a τ value of 0.18 and 0.14, respectively [τ = 170.25–159.31)/60 = 0.18 for Cu1 and (171.08–162.48)/60 = 0.14 for Cu2]. The τ values clearly indicate that the copper atoms in **3** are in a five coordinate, slight distorted square pyramidal environment [69].

The pzdc ligand adopts tridentate and tetradentate coordination modes to connect Cu(II) centers. One of the pzdc ligand bridges three copper atoms to form a tetranuclear unit. At the same time the other pzdc ligand bridges two copper atoms from the two adjacent complex molecules to get a 1D double-chain motif. The adjacent Cu1···Cu1^i, Cu1···Cu2^i and Cu2···Cu2^{ii} distances in the chain are 6.827 Å, 5.173 and 6.471 Å, respectively ((i) $2-x$, $1-y$, $-z$; (ii) $2-x$, $2-y$, $-1-z$).

The most interesting feature of this structure is the presence of C–H···Cu close hydrogen bonding interactions between the Cu2 centers and H atoms of methyl group identified by X-ray diffraction (Fig. 6). These weak interactions have facilitated the formation of the coordination bond between Cu1 and 2-meim ligand. The bond distance (H10A···Cu2) and angle (C10–H10A···Cu2) are 3.014 Å and 132.17°, respectively. To the best of our knowledge, such arrangements are rarely presented up to now [72,73].

The 1D chains of **3** are further joined together by O–H···O, N–H···N and N–H···O hydrogen bonds between the uncoordinated water molecules/2-meim nitrogen atoms and the carboxyl oxygen/pyrazine nitrogen atoms from pzdc ligands to form the 3D frameworks (Fig. 7a) containing 1D channels constructed by the cooperative association of covalent and hydrogen bonds (Fig. 7b). The PLATON program analysis showed that unit cell contains some voids and that the total potential solvent volume is 163.0 Å^3, or

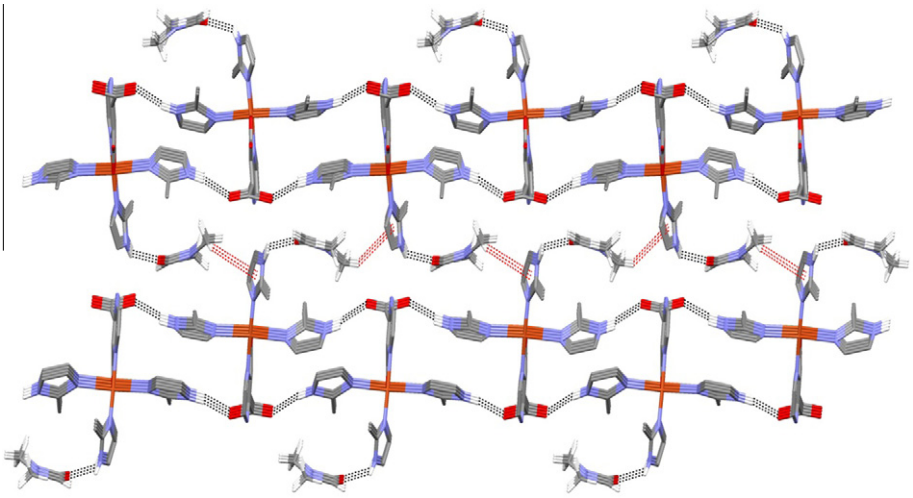

Fig. 4. Intra- and intermolecular hydrogen-bonding geometry and C–H···π interactions of **2**.

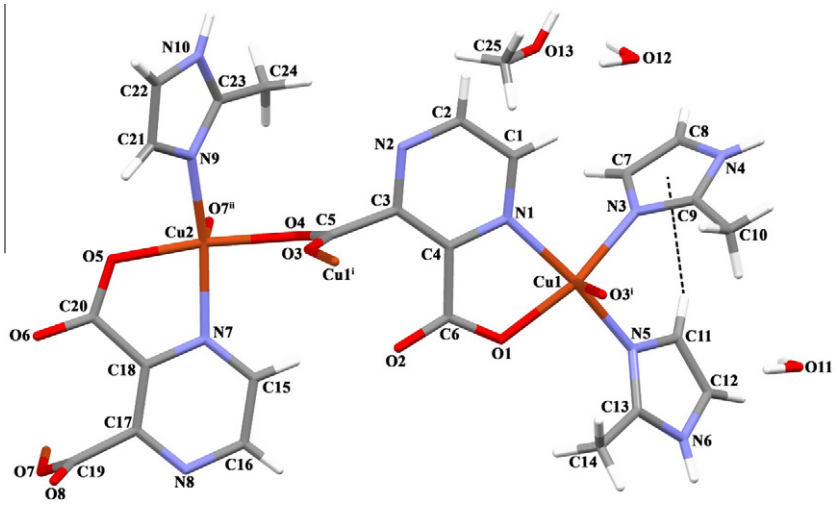

Fig. 5. Molecular structure of $\{[Cu(\mu_3\text{-pzdc})(2\text{-meim})_2Cu(\mu\text{-pzdc})(2\text{-meim})]\cdot CH_3OH\cdot 2H_2O\}_n$ (**3**) with atom-labeling scheme. (i) $2-x, 1-y, -z$; (ii) $2-x, 2-y, -1-z$.

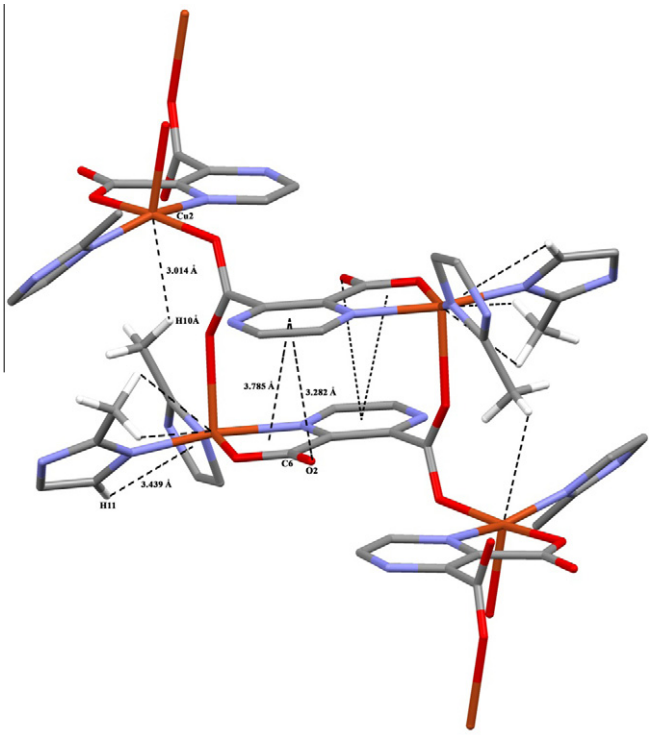

Fig. 6. C–H···Cu(II) and C=O···π interactions of **5**.

9.6% [74]. The two lattice water molecules and one methanol molecule act as guest molecules in these cavities along the *a* axis (Fig. 7a). Furthermore, there are C=O···π and C–H···π interactions between C6=O2, C20=O6, C11–H11 and pyridine (Cg1 and Cg2), imidazole (Cg3) rings (Cg1=N1–C1–C2–N2–C3, Cg2=N7–C15–C16–N8–C17 and Cg3=N3–C7–C8–N4–C9; C6=O2···Cg1 = 3.282 Å, C20=O6···Cg2 = 3.393 Å and C11–H11···Cg3 = 3.440 Å), resulting in a three-dimensional (3D) supramolecular framework (Fig. 7a).

3.4. $[Zn(\mu\text{-pzdc})(H_2O)_3]_n$ (**4**)

The X-ray crystallographic analysis shows that **4** crystallizes in the monoclinic space group $P2_1/c$ and has an infinite 1D chain structure. As shown in Fig. 8, a crystallographically independent Zn(II) ion is surrounded with a distorted octahedral geometry by three aqua ligand, two carboxyl oxygen atoms (O1 and $O4^i$) and one nitrogen atoms (N2) from two pzdc ligands [average Zn1–O = 2.071 and Zn2–N2 = 2.145(2) Å]. These bond distances are similar to the corresponding values found in $[Zn(pzdc)(H_2O)_2]\cdot H_2O$ [45], $\{[Zn(\mu\text{-pzdc})(H_2O)_3]\cdot H_2O\}_n$ [46], $\{(H_3O)_2[Zn(\mu\text{-pzdc})_2]\}_n$ [38] and $[Zn_2(pzdc)_2(H_2O)_4]\cdot 2.5H_2O$[40] but somewhat shorter than that in $\{[Zn(\mu\text{-Hpzdc})(H_2O)_2]\cdot NO_3\}_n$ [41], $[Zn(\mu\text{-pzdc})(H_2O)_3]\cdot H_2O$[40]. The deprotonated pzdc are μ-bridging ligands and they join the neighboring Zn(II) ions to form this one-dimensional linear chain structure along *b* axis.

The hydrogen bonding geometries are given in Table 3. The crystal packing analysis indicate that the crystal packing of **4** is formed via intermolecular hydrogen bonding and C=O···π interactions (Fig. 9). The adjacent chains are further aggregated into a three-dimension (3D) network through the hydrogen bonds between the aqua ligand, carboxylate oxygen atoms and pyrazine nitrogen atom (Fig. 7b). The C=O···π interactions also exist in the adjacent 1D chains between C6=O3 and pyrazine ring (Cg1) (Cg1=N1, N2, C1, C2, C3, C4 and O3···Cg1=3.298 Å) (Fig. 7a).

3.5. $\{[Zn(\mu\text{-pzdc})(NH_3)_2(H_2O)]\cdot H_2O\}_n$ (**5**)

As illustrated in Fig. 10, Zn1 atom in **5** is coordinated by two carboxyl oxygen atoms (O1 and $O4^i$) and one nitrogen atoms (N1) from two pzdc ligands, two nitrogen atoms from two amine ligands and one oxygen atom from aqua ligand, giving a slightly distorted octahedral geometry. The equatorial plane is formed by O1, $O4^i$, N1 and N4 atoms, while the axial positions are occupied by O5 and N3 atoms. The complex contains 1D chain, containing ZnN_3O_3 units with pzdc as bridging ligand (Fig. 10). The adjacent Zn···Zn distance in the complex chain is 7.720 Å.

The crystal packing of the complex is stabilized by inter-molecular hydrogen bonding and N–H···π interactions (Fig. 11). In crystal, the adjacent chains are connected through N–H···O hydrogen bonds from carboxyl oxygen atom, aqua and amine ligands, leading to 2D layer in *bc* plane (Fig. 11b). Furthermore, there is also N–H···π interaction between N3–H3B and pyrazine ring (Cg1) (Cg1=N1, C1, C2, N2, C3, C4 and H3B···Cg1 = 3.303 Å) (Fig. 11a). Adjacent 2D layers stacked one another through the hydrogen bonding interactions ($N3\cdots N2^{iv}$ = 3.227 (3), $N4\cdots O2^{ii}$ = 2.929 (2), $N4\cdots O1^{vi}$ = 3.020 (2) and $O5\cdots O2^{v}$ = 2.780 (2) Å), giving rise to a three-dimensional supramolecular architecture.

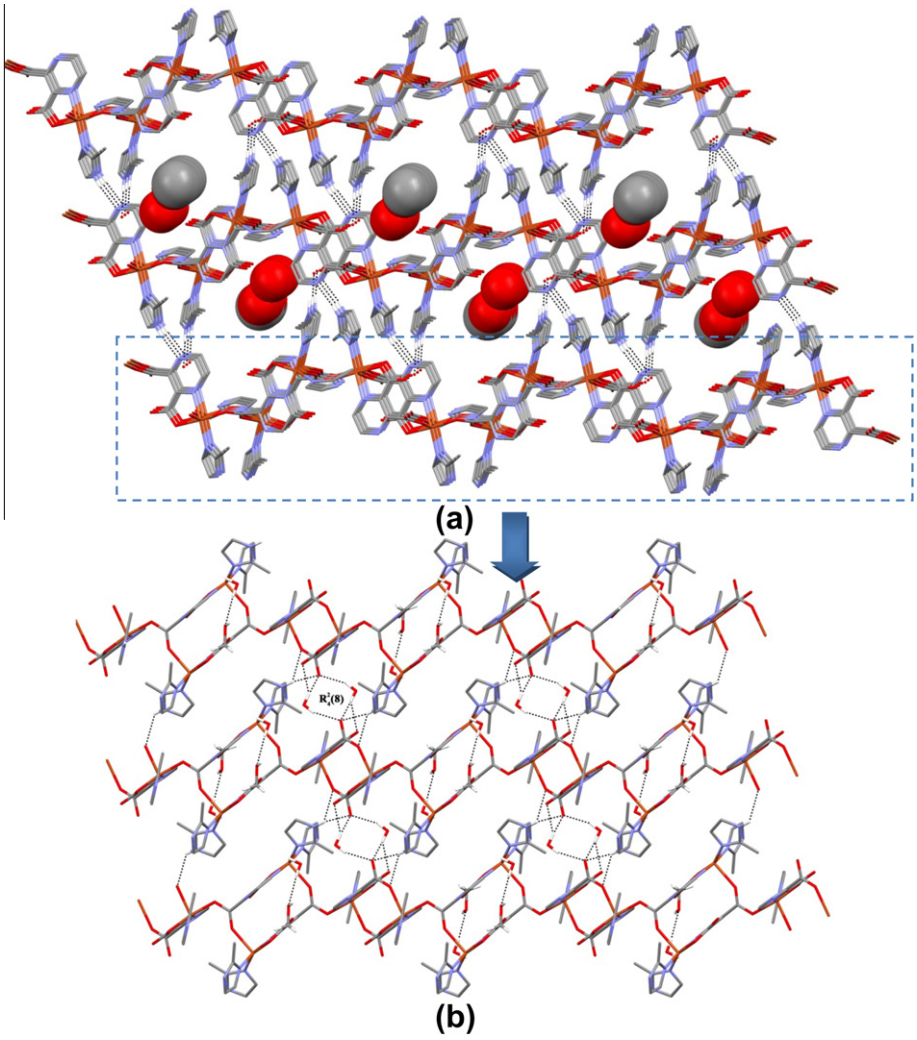

Fig. 7. (a) 3-D supramolecular network filled with water and CH_3OH molecules along the *a* axis in **3**. (b) Hydrogen bonds geometry for **3**. Dashed lines are hydrogen bonds. Non-H bonding H atoms omitted for clarity.

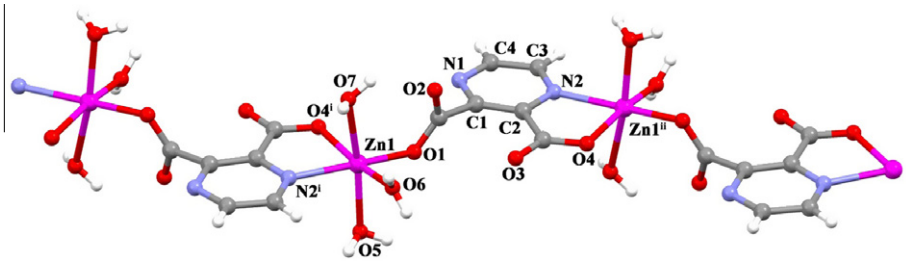

Fig. 8. Molecular structure of $[Zn(\mu\text{-pzdc})(H_2O)_3]_n$ (**4**) with atom-labeling scheme (symmetry codes: (i) $1-x, -1/2+y, 1.5-z$; (ii) $1-x, 1/2+y, 1.5-z$).

3.6. *{[Cd(μ-pzdc)(im)$_3$]·0.13H$_2$O}$_n$* (**6**)

The crystal structure of the complex **6** with the atom labeling is shown in Fig. 12. The asymmetric unit contains one six-coordinated Cd(II) atom, one 2,3-pzdc ligand, three im ligands and 0.13 crystal water molecule. Single crystal X-ray analysis showed that complex **6** exhibits one-dimensional zigzag chain running along the crystallographic *b*-axis direction. Each cadmium atom is coordinated in a distorted octahedral geometry, which is defined by one N atom and two O atoms from two pzdc ligands and three N atoms from three im ligands. Two O atoms of carboxylate group (O1 and $O2^{ii}$) and two N atoms (N1 and N5) comprise the equatorial plane, while two N atoms occupy the axial position. The pzdc ligand coordinated to the Cd(II) atom in a μ-(κ^3N,O^2:O$^{2'}$) mode (Scheme 1d). The carboxylate group in the 3-position is almost perpendicular to the pyrazine ring plane because of steric interaction between the two carboxylate groups and remains uncoordinated. This coordination mode of pzdc ligand is quite uncommon [49].

The carboxylate groups, C5/O1/O2 and C2/O3/O4, are twisted from their attached pyrazine planes (N1/N2/C1–C4), with dihedral angles of 20.94 and 74.77°, respectively. The dihedral angle between two carboxylate groups is 66.37°. Similar distortions of the

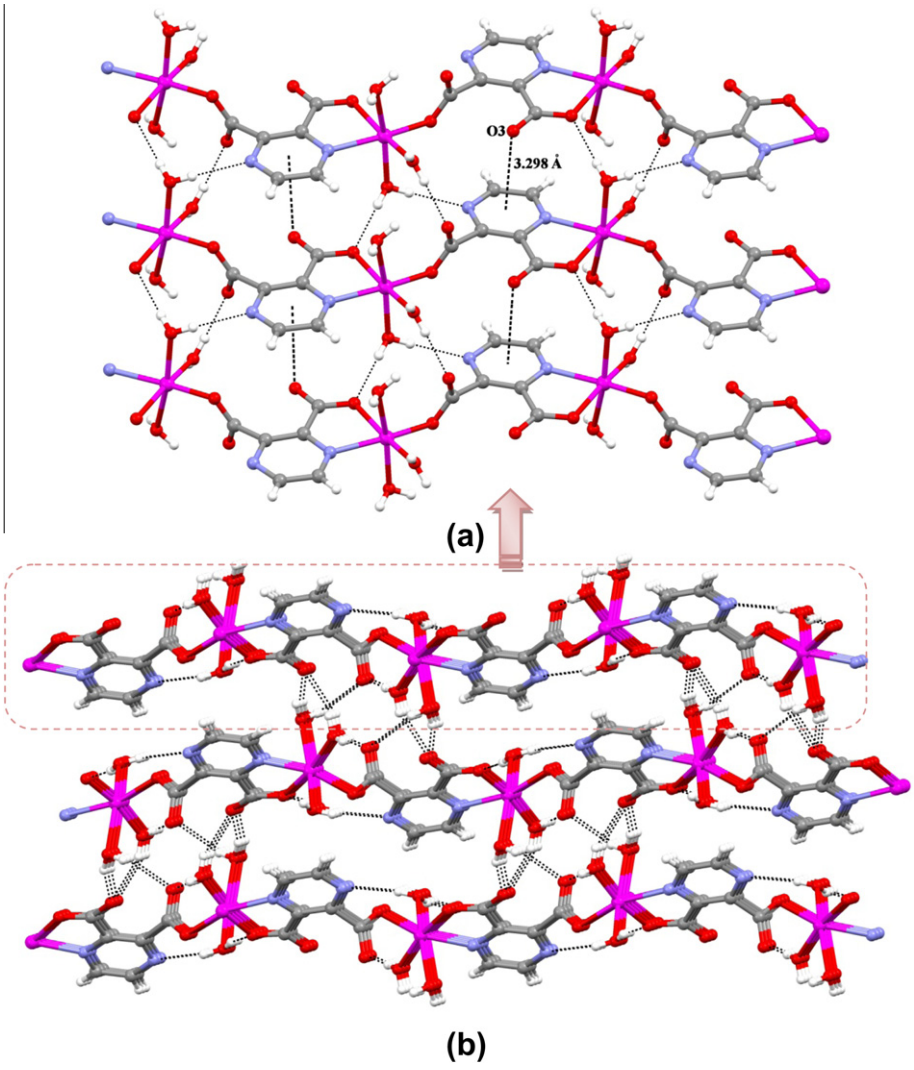

Fig. 9. C=O···π and hydrogen-bonding interaction between the chains (a) and layers (b) of **4**.

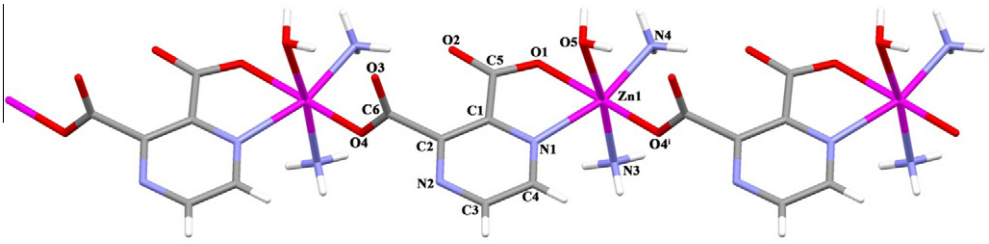

Fig. 10. Molecular structure of $[Zn(\mu\text{-pzdc})(NH_3)_2(H_2O)]_n$ (**5**) with atom-labeling scheme (symmetry code: (i) 1 + *x*, *y*, 1 + *z*).

ligand are observed in some pzdc complexes [4,35,75]. The Cd(1)···Cd(1)^{i} distances in the chain is 5.227 Å, while between chains distance Cd(1)···Cd(1)^{ii} is 9.254 Å.

The crystal packing of complex is a composite of π···π, C–H···π and hydrogen bonding interactions. Within each chain, two adjacent pyrazine and imidazole rings are involved in the π···π stacking interactions with the closest centroid distance between pyrazine and imidazole rings 3.7491 Å (Fig. 13a), while C–H···π interaction take place between C(11)–H(11)···Cg3^{ii} for **6** (Cg3=N(3)–C(7)–N(4)–C(8)–C(9), 2.78(2) Å, (ii): ½ − *x*, ½ − *y*, −*z*] (Fig. 13b). The crystal structure is stabilized through strong intermolecular hydrogen bonding between N atoms of imidazole ligands and O atoms of carboxylate groups to form a 2D network and generate the $R_3^3(21)$ and $R_5^4(40)$ motifs (Fig. 14). The water molecule is also involved in interchain hydrogen bonding with the carboxyl oxygen atom [O5···O4 = 2.727 (9) Å] and this hydrogen bond is nearly linear (170(4)°). All of these intermolecular interactions give a three-dimensional framework (Fig. 15).

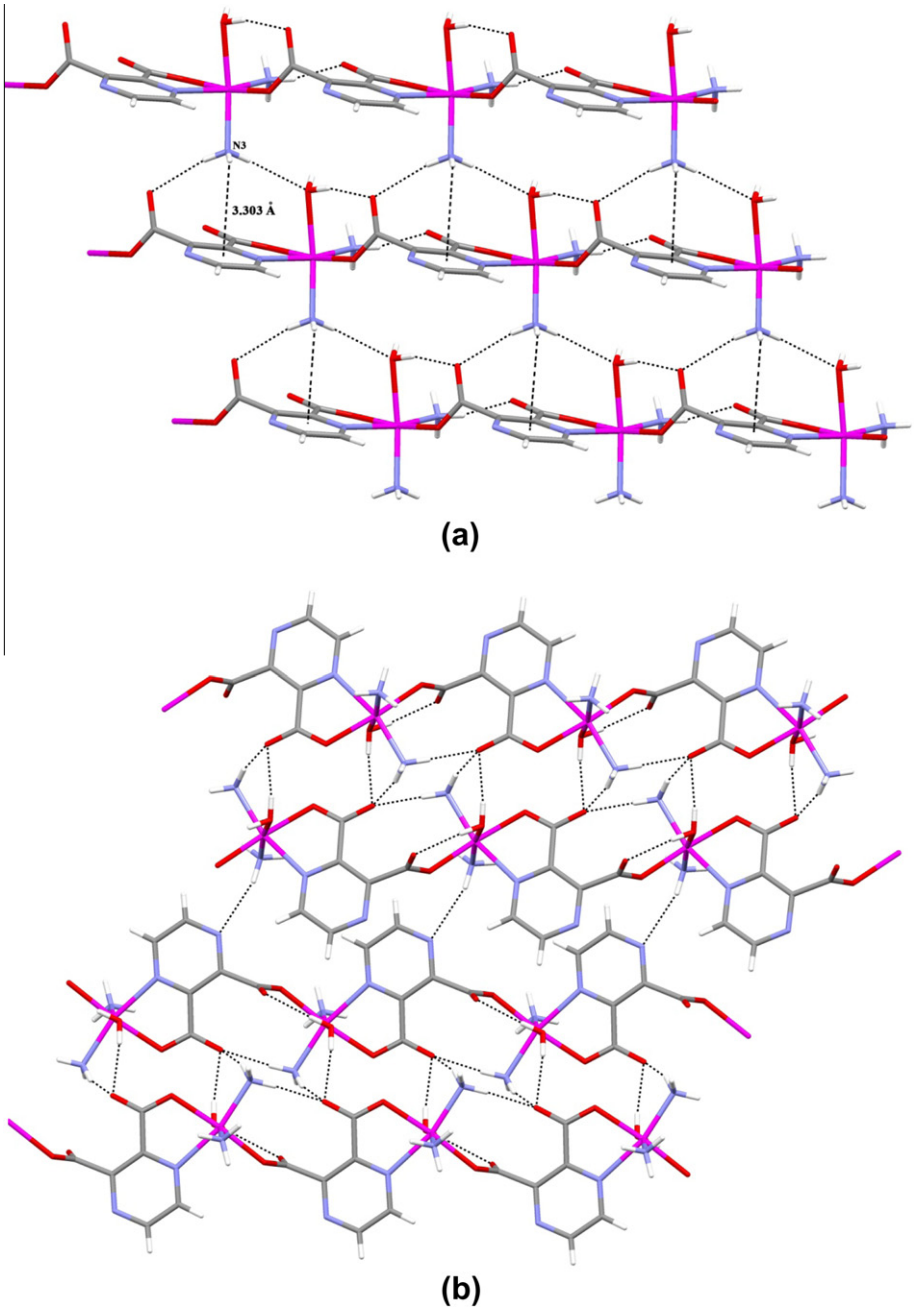

Fig. 11. C=H···π (a) and hydrogen-bonding interaction (b) between the chains of **5**.

*3.6.1. {[Cd(μ-pzdc)(N-mim)$_3$]·3H$_2$O}$_n$ (**7**)*

Complex **7** is similar to complex **6**. The asymmetric unit consists of one Cd(II) atom, one pzdc and three 2-meim ligands. The Cd atom is six-coordinate and has a distorted octahedral geometry, formed by two carboxylate O atoms and one pyrazine N atom from two pzdc ligands, three N atoms from three *mer*-oriented 2-meim ligands (Fig. 16).

The coordination mode adopted by the pzdc ligand can be classified as μ-($\kappa^3N,O^2:O^3$), that is, a 2-position carboxylate O atom and the pyrazine N atom chelate one Cd(II) atom and a 3-position carboxylate O atom binds to another Cd(II) atom (Scheme 1a). This coordination mode of pzdc ligand is the first sample for Cd(II) atom. The dihedral angle between the pyrazine ring and the O3/C5/O4 O1/C6/O2 carboxylate group is 63.85° and 25.21°, respectively. The Cd(II) ions are linked by the pzdc ligands into an infinite [Cd(μ-pzdc)(N-mim)$_3$]$_n$ zigzag chain along the [0 1 0] direction, with a shorter Cd···Cd distance of 7.959 Å.The C–H···π interactions between the C10–H10A and imidazole ring [Cg1 = N5–C11–N6–C13–C12; H10A···Cg1 = 3.797 Å and C10–H···Cg10A = 159°] in different chains connect the one-dimensional chains to form a two-dimensional layer with the nearest Cd···Cd distance in adjacent chains of 9.419 Å (Fig. 17). The hydrogen bonding interactions between the crystal water molecule and the uncoordinated carboxyl oxygen atoms of pzdc ligand further connect the two-dimensional layers to generate a three-dimensional supramolecular architecture. Two lattice water molecules are hydrogen bonded to each other to generate an acyclic D3 water cluster. These clusters are interacting with the

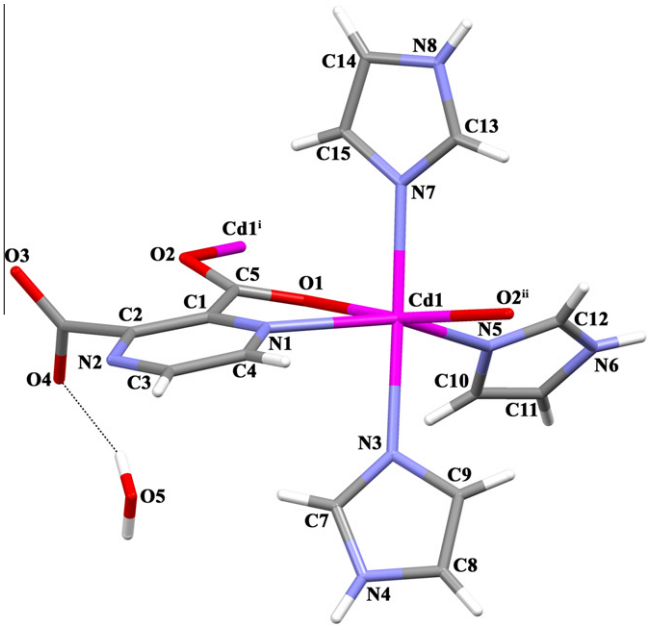

Fig. 12. The molecular structure of $\{[Cd(\mu\text{-pzdc})(im)_3]\cdot 0.13H_2O\}_n$ (**6**) with atom-labelling scheme.

uncoordinated carboxyl oxygen atoms, forming a tape-like infinite patterns in which two eight-($R_4^4(8)$) and twelve-membered ($R_6^4(12)$) rings are observed [76] (Fig. 18).

3.6.2. $[Cd(\mu\text{-pzdc})(2\text{-meim})_3]_n$ (**8**)

The molecular structure with atomic numbering scheme of complex **8** is shown in Fig. 19. X-ray crystal structure analysis reveals that the complex **8** consists of 1-D polymeric chain, elongated along axis *c* (Fig. 20). The Cd(1) atom is coordinated by two oxygen atoms O1, $O2^i$, one nitrogen atom N1 from two pzdc ligands, three nitrogen atoms N3, N5 and N7 of the 2-meim ligands, having a distorted octahedral coordination. The pzdc ligand is coordinated to one Cd(II) ion through its one carboxyl oxygen and one pyrazine nitrogen atom, and coordinated to the other Cd(II) ion through another carboxyl oxygen atom (Scheme 1a). The adjacent Cd–Cd distance in the chain is 5.491 Å. The carboxyl group coordinated of pzdc and pyrazine ring are almost parallel as the dihedral angle between them is 2.73°, while the carboxyl group uncoordinated and the pyrazine ring are approximately vertical as the dihedral angle between them is 83.62°.

The adjacent chains interact with each other through π···π stacking between imidazole ring, with a separation of 3.879 Å and interchain N–H···O interactions involving the hydrogen atom of 2-meim ligand and the O atom of the carboxylate group of pzdc ligand in the lattice (Fig. 20). The 2D layers are connected together

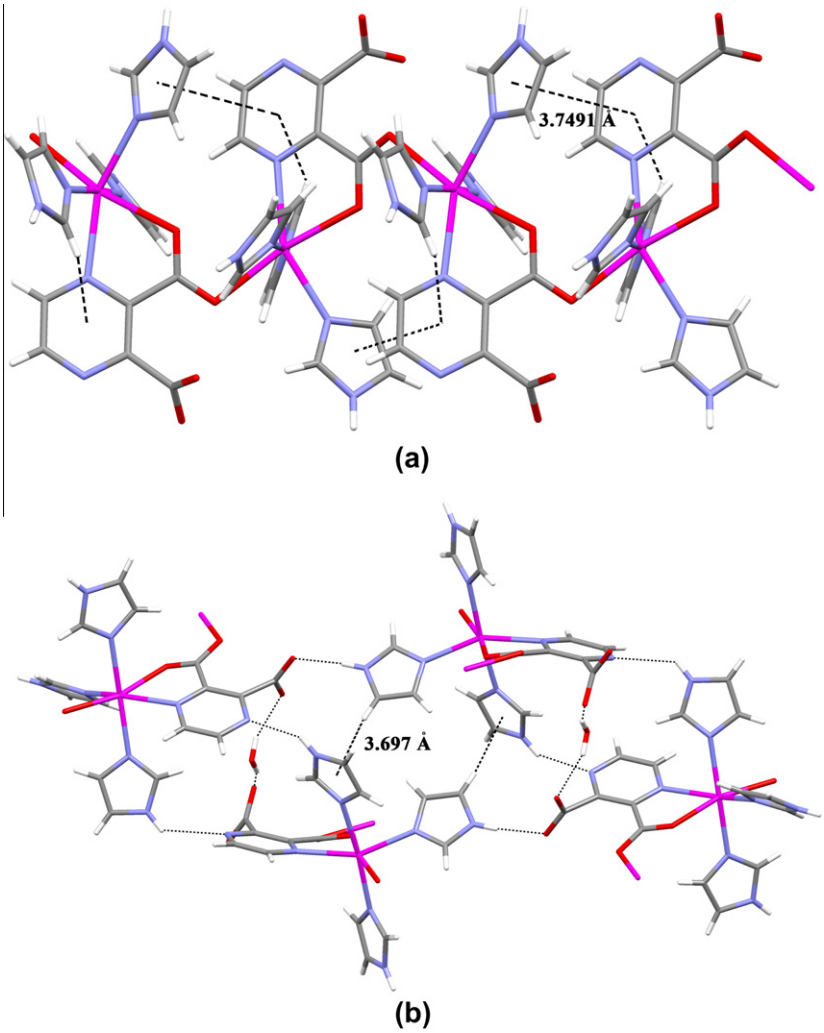

Fig. 13. The C–H···π, π···π (a) and hydrogen bonding interactions (b) of **6**.

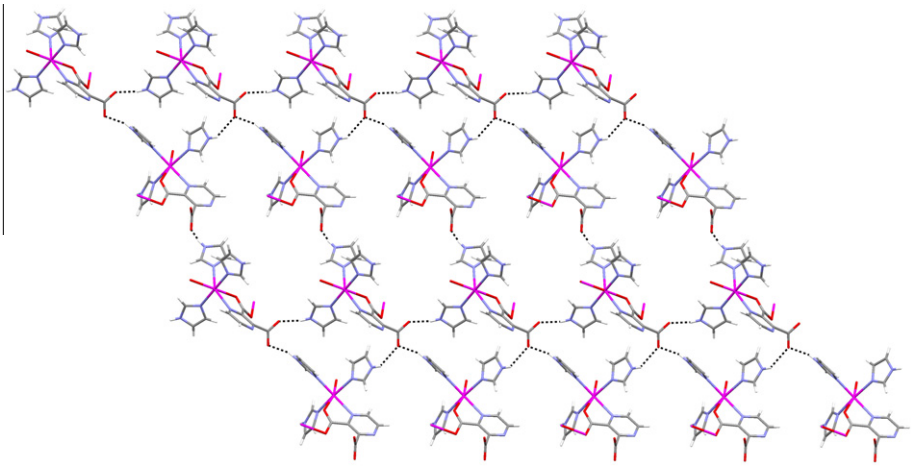

Fig. 14. A view of the 2D network of **6**, showing the $R_3^3(21)$ and $R_5^4(40)$ ring patterns.

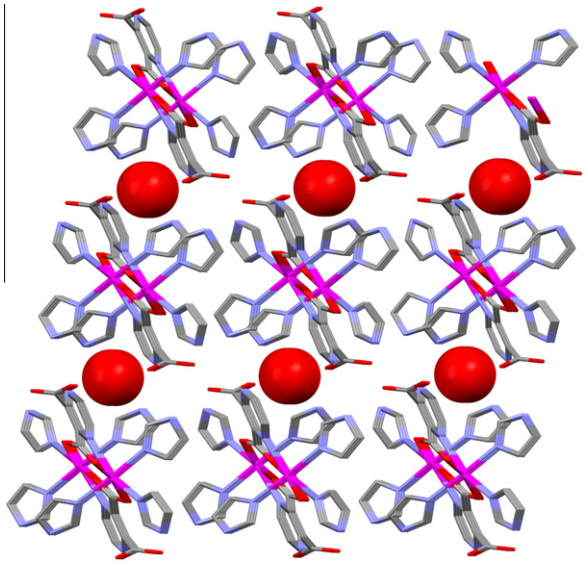

Fig. 15. 3-D supramolecular network filled with water molecules in **6**.

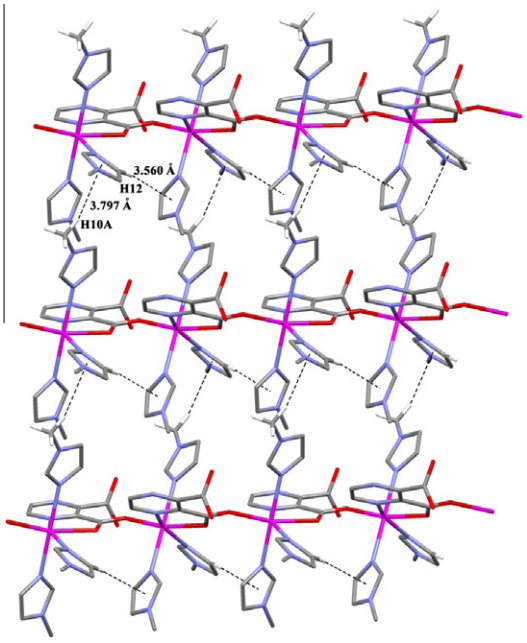

Fig. 17. C–H···π interaction between the chains of **7**.

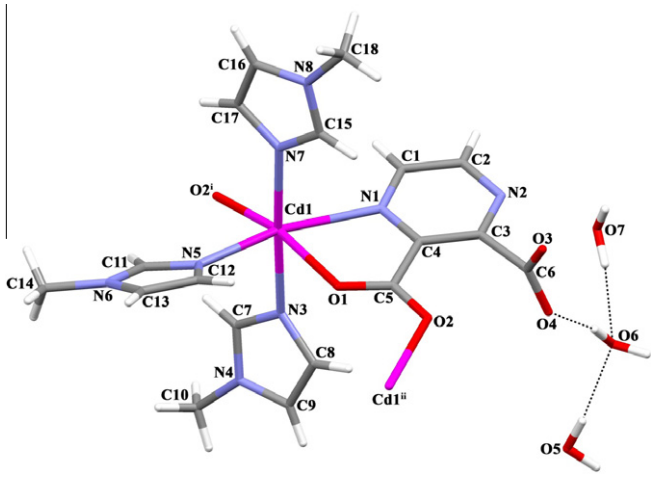

Fig. 16. Molecular structure of $\{[Cd(\mu\text{-pzdc})(N\text{-mim})_3]\cdot 3H_2O\}_n$ (**7**) with atom-labeling scheme.

through N–H···O hydrogen bonding interaction resulting in a three-dimensional framework.

4. Results of molecular simulations

We predicted H_2 uptake capacities of synthesized complexes using GCMC simulations in order to assess the potential of these materials for H_2 storage. Fig. 21 shows the single component adsorption isotherms of H_2 in complexes at 298 K as a function of fugacity. In all molecular simulations, the bulk phase composition was specified in terms of fugacity since the differences between fugacity and pressure for H_2 for the conditions considered here are small. The adsorption capacities of **1** and **8** exceed 2 mg H_2/g material at pressures above 20 bar at room temperature whereas the H_2 uptake capacities of other materials are less than 1 mg H_2/g material. We also compared the H_2 storage capacities of the complexes synthesized in this work with other well known nanoporous materials in Table 5. Material **1** has a better storage

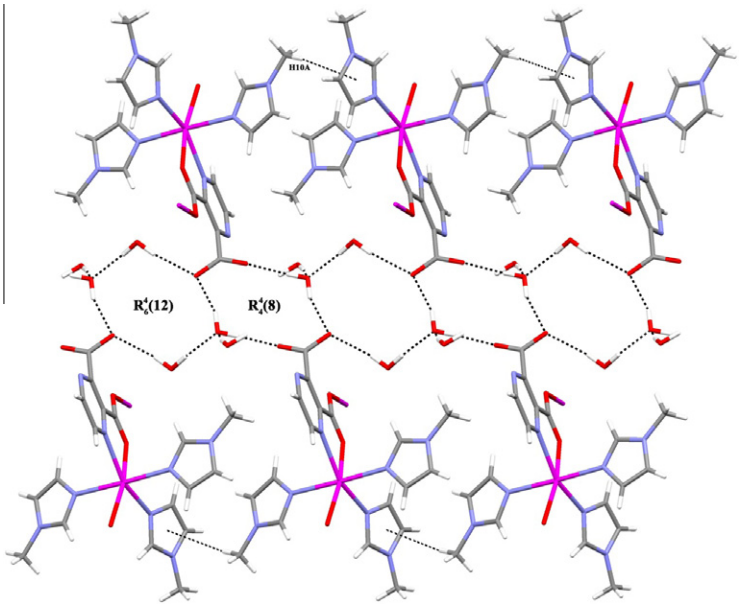

Fig. 18. View of $R_6^4(12)$ and $R_4^4(8)$ motifs and the D3 water cluster extended through a carboxylate oxygen atoms.

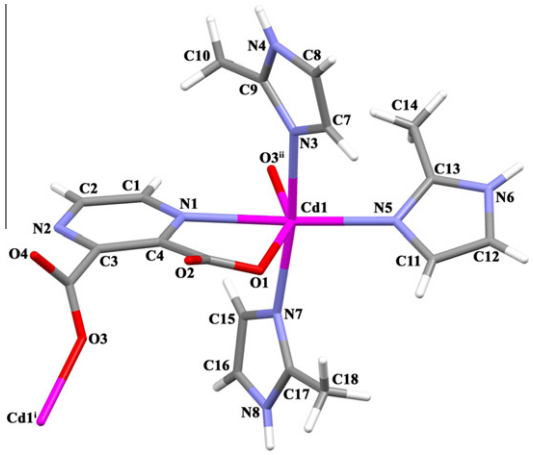

Fig. 19. The molecular structure of $[Cd(\mu\text{-pzdc})(2\text{-meim})_3]_n$ (**8**) with atom-labeling scheme.

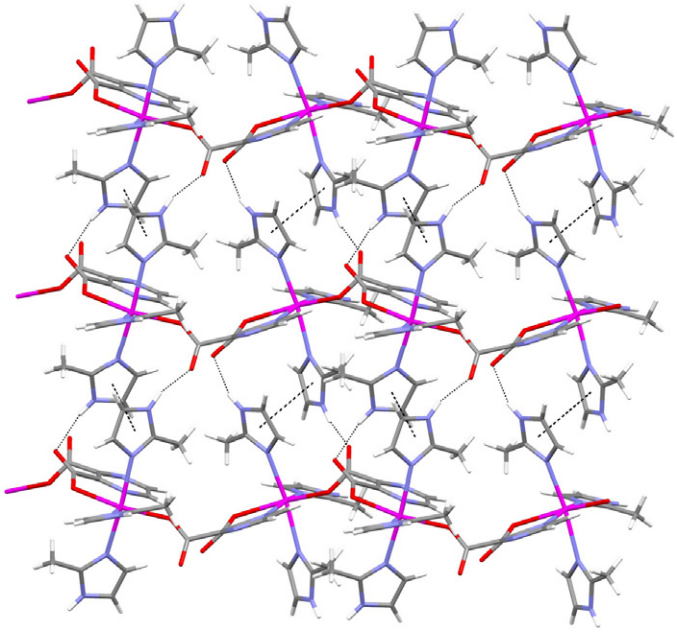

Fig. 20. The π···π and hydrogen bonding interactions of **8**.

capacity than multi-walled carbon nanotubes under the same conditions and its capacity is comparable to those of single walled carbon nanotubes and carbon nanofibers. MOF-5 and Cu(hfipbb)$(H_2$hfipbb$)_{0.5}$ are the two widely studied materials for H_2 storage in the literature and they exhibit higher H_2 adsorption capacities due to their large pore sizes.

5. Antimicrobial activities

The results are presented in Table 6 as minimum inhibitor concentration (MIC) values (μg/mL) which is the minimum concentration to inhibit the growth of bacteria or yeast. The value of MIC indicates that the antimicrobial activity of **7** was in the range of 10–60 μg/mL concentration in studied microorganisms. While pyrazine-2,3-dicarboxylic acid showed activity at high concentrations on studied microorganisms (625–1250 μg/mL), antimicrobial activity of **2** is higher than H_2pzdc. It is shown that the effectiveness of **2** and **7** is same on gram (−) and gram (+) bacteria. Especially, complex **7** was more effective on *P. aeruginosa, S. aureus* and MRKNS. Clinical isolates were generally more resistant than wild type bacteria against new synthesized complexes.

The biological effect of various pzdc metal complexes was demonstrated in different studies [77–79]. It is reported that pyrazine-2,3-dicarboxylic acid derivatives are a candidate for *Mycobacterium tuberculosis* [80]. The focus point of the production of antimicrobial agents is to reveal a complex which will stop different targets of bacteria but not harm the host. Metal complexes are very interesting materials in this regard. Biocations such as Co(II), Ni(II), Cu(II), Fe(III), Cr(III), Mn(III), Zn(II) and metal ions such as Cd(II), Pd(II), Pt(II), Ag(I) was found to have very high activity inhibit development of bacterial resistance [79]. We can

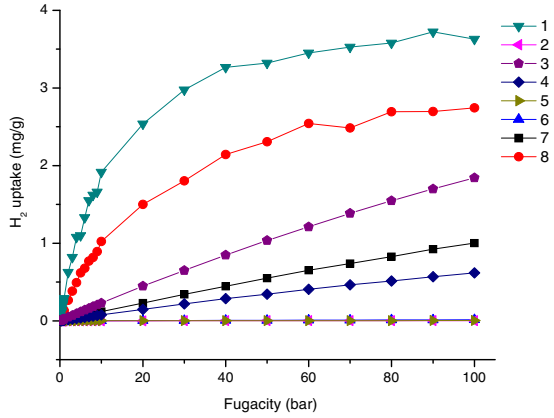

Fig. 21. Predicted H_2 uptake capacity of complexes at 298 K computed from GCMC simulations as a function of fugacity.

propose that the new metal complex **7** can be used for staphylococcal infections.

6. Photoluminescent properties

The photoluminescent properties of H_2pzdc and complexes **4–8** were investigated at room temperature. The emission spectra of complexes **4–8** are shown in Fig. 22. The H_2pzdc displays photoluminescence with emission maxima at 412 nm ($\lambda_{ex.}$ = 286 nm). It can be presumed that this peak originate from the $\pi^* \rightarrow n$ or $\pi^* \rightarrow \pi$ transition. The complex **4** exhibits green and yellow radiation emission maxima at 532 nm and 584 nm upon photoexcitation at 387 nm. Whereas, it can be observed that the blue emission for complexes **5–8** occur at 466, 521, 424 and 418 nm with upon excitation at 384, 376, 285 and 289 nm, respectively. The emissions of 5, 6 and 7, 8 may be assigned to the ligand-to-metal charge-transfer bands (LMCT) and ligand-centered transition, respectively [81].

Table 5
Comparison of H_2 storage capacity of the materials studied in this work with other nanoporous materials. Data for materials except **1** and **8** were taken from Ref. [82].

Materials	H_2 storage (wt.%)	T (K)	P (bar)
$[Cd(\mu\text{-pzdc})(2\text{-meim})_3]_n$	0.27	298	100
Carbon nanotube (multi)	<0.3	298	100
$[Co(\mu\text{-pzdc})(H_2O)(2\text{-meim})_2]_n$	0.36	298	100
Carbon nanotube (single)	0.5	298	1
Carbon nanofiber	0.7	293	100
$[Cu(hfipbb)(H_2hfipbb)_{0.5}]$	1.0	298	48
MOF-5	1.6	298	10

Table 6
The MIC values of new complexes on some wild type and clinical isolates microorganisms (μg/mL).

Compounds	Wild type					Clinic isolates					
	E. coli	*S. aureus*	*B. cereus*	*P. aeruginosa*	*C. albicans*	*E. coli*	MRSA	MRKNS	*A. baumanni*	*M. morganii*	*E. aerogenes*
2	1000	1000	1000	1000	2000	NT	NT	NT	NT	NT	NT
7	60	20	60	10	20	70	44	2.75	175	175	175
H_2pzdc	625	625	625	625	625	1250	1250	625	1250	1250	1250

New complexes $[Co(\mu\text{-pzdk})(H_2O)(2\text{-mim})_2]_n$ (**1**), $\{[Cu(\mu_3\text{-pzdk})(2\text{-mim})_2Cu(\mu\text{-pzdk})(2\text{-mim})]\cdot CH_3OH\cdot 2H_2O\}_n$ (**3**), $[Zn(\mu\text{-pzdk})(H_2O)_3]_n$ (**4**), $[Zn(\mu\text{-pzdk})(NH_3)_2(H_2O)]\cdot H_2O\}_n$ (**5**), $[Cd(pzdk)(im)_3]\cdot 0{,}13H_2O$ (**6**) and $[Cd(\mu\text{-pzdk})(2\text{-mim})_3]_n$ (**8**) did not dissolve in ethanol, pure water, DMSO and methanol.

Table 7
Thermoanalytical results (TG, DTG and DTA) of complexes.

Complexes	Decomposition		$DTG_{max.}$ (°C)	Remove group	Mass loss (%)		Total mass loss (%)		Proposed decomposition product
	Stage	Temp. range (°C)			Calc.	Found	Calc.	Found	
$[Co(\mu\text{-pzdc})(H_2O)(2\text{-meim})_2]_n$	1	173–238	212(+)	H_2O + 2-meim	24.57	26.15	80.27	84.24	[Co(pzdc)(2-meim)]
(1)	2	238–446	393(−)	(2-meim)+pzdc	55.71	58.09			Co_3O_4
$[Cu(pzdc)(2\text{-meim})_3]\cdot DMF$	1	86–193	157(+)	DMF	13.30	13.69	85.4	85.9	$[Cu(pzdc)(2\text{-meim})_3]$
(2)	2–4	193–445	222(+), 241(−), 353(−), 430(−)	3(2-meim) + pzdc	72.17	72.29			CuO
$\{[Cu(\mu_3\text{-pzdc})(2\text{-meim})_2Cu(\mu\text{-pzdc})(2\text{-meim})]\cdot CH_3OH\cdot 2H_2O\}_n$	1	83–207	99(+)	$2H_2O + CH_3OH$	8.79	8.16	79.41	80.41	$[Cu(pzdc)(2\text{-meim})_2Cu(pzdc)(2\text{-meim})]$
(3)	2–4	207–462	222(+), 236(+), 432(−)	3(2-meim) + 2pzdc	70.62	72.25			2CuO
$[Zn(\mu\text{-pzdc})(H_2O)_3]_n$	1	84–185	133(+)	$3H_2O$	18.91	17.17	71.49	71.92	[Zn(pzdc)]
(4)	2,3	185–502	227(+), 327(−), 459(−)	pzdc	52.58	54.75			ZnO
$\{[Zn(\mu\text{-pzdc})(NH_3)_2(H_2O)]\cdot H_2O\}_n$	1	99–286	180.31(+)	$2H_2O + 2NH_3$	24.70	21.41	71.28	74.11	[Zn(pzdc)]
(5)	2,3	286–548	328(−), 489(−)	pzdc	52.93	53.39			ZnO
$[Cd(pzdc)(im)_3]\cdot 0.13H_2O$	1	30–45	43(+)	$0.13H_2O$	0.48	0.52	73.52	71.69	$[Cd(pzdc)(im)_3]$
(6)	2,3	225–284	232(+), 269(+)	im	28.07	28.95			$[Cd(pzdc)(im)_2]$
	4,5	284–532	303(+), 526(−)	2im + pzdc	44.97	42.22			CdO

(*continued on next page*)

Table 7 (*continued*)

Complexes	Decomposition		$DTG_{max.}$ (°C)	Remove group	Mass loss (%)		Total mass loss (%)		Proposed decomposition product
	Stage	Temp. range (°C)			Calc.	Found	Calc.	Found	
$\{[Cd(\mu\text{-pzdc})(N\text{-mim})_3].3H_2O\}_n$	1	61–108	99(+)	$3H_2O$	9.32	9.81	77.81	78.40	$[Cd(pzdc)(N\text{-mim})_3]$
(7)	2	108–159	147(+)	N-mim	14.18	12.17			$[Cd(pzdc)(N\text{-mim})_2]$
	3,4	159–489	249(+), 480(−)	2(N-mim) + pzdc	54.30	56.42			CdO
$\{[Cd(pzdc)(2\text{-meim})_3]\}_n$	1–3	128–368	172(+), 279(+),	3(2-meim)	45.62	45.53	73.42	72.23	$[Cd(pzdc)(2\text{-me im})_3]$
(8)	4,5	455–521	318(+) 428(−), 504(−)	pzdc	27.80	26.70			$[Cd(pzdc)]$ CdO

* (+) Endothermic, (−) exothermic.

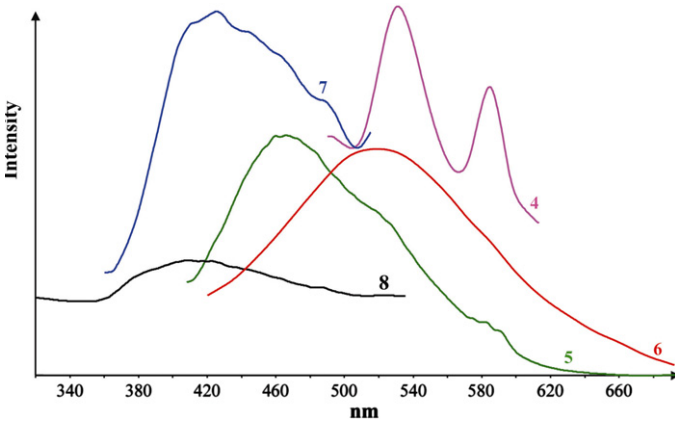

Fig. 22. Solid state emission spectra of complexes **4**–**8** at room temperature.

7. Thermal analyses

Thermal decomposition behaviors and stability of all complexes were studied in static atmosphere of air in the temperature range 30–700 °C. All complexes begin to decompose without melting and exhibit similar decomposition characteristics. In the first stage, endothermic removal of the water, amine and solvent molecules take place in the temperature range 30–286 °C. This stage is followed by partially or complete decomposition of the imidazole derivatives and/or pzdc ligands. In the later stage, the remaining organic residue exothermically burns. The final decomposition products which were identified by IR spectroscopy were the corresponding metal oxides. Thermoanalytical results (TG, DTG and DTA) on the complexes are summarized in Table 7.

8. Conclusions

Eight pyrazine-2,3-dicarboxylate complexes with N-donor ligands have been synthesized and characterized. The results in this study clearly show that the pzdc ligand exhibits four different coordination modes in the presence of im, N-meim and 2-meim ligands. Furthermore, some of the compounds in this study shows that solvents plays an important role in the construction of discrete coordination architectures. In addition, the interesting feature of this study is the presence of C–H···Cu close hydrogen bonding interactions between the Cu center and H atoms of methyl group identified by X-ray diffraction. Moreover, the photoluminescence properties of compounds **4–8** have been examined.

Acknowledgements

This work has been supported by The Scientific and Technological Research Council of Turkey (TUBITAK, No: 109T201).

Appendix A. Supplementary material

CCDC 806249, 819383, 819384, 827827, 819385, 693907, 819386 and 806248 contain the supplementary crystallographic data for this paper. These data can be obtained free of charge from The Cambridge Crystallographic Data Centre via www.ccdc.cam.ac.uk/data_request/cif.

References

[1] O.M. Yaghi, H.L. Li, C. Davis, D. Richardson, T.L. Groy, Acc. Chem. Res. 31 (1998) 474.
[2] P.J. Hagrman, D. Hagrman, J. Zubieta, Angew. Chem., Int. Ed. 38 (1999) 2639.
[3] B. Moulton, M.J. Zaworotko, Chem. Rev. 101 (2001) 1629.
[4] H. Yin, S.X. Liu, Polyhedron 26 (2007) 3103.
[5] C. Janiak, Dalton Trans. (2003) 2781.
[6] C. Janiak, Angew. Chem., Int. Ed. 36 (1997) 1431.
[7] S.L. James, Chem. Soc. Rev. 32 (2003) 276.
[8] S.L. Zheng, X.M. Chen, Aust. J. Chem. 57 (2004) 703.
[9] M. Eddaoudi, J. Kim, D. Vodak, A. Sudik, J. Wachter, M. O'Keeffe, O.M. Yaghi, Proc. Natl. Acad. Sci. U.S.A. 99 (2002) 4900.
[10] D. Maspoch, D. Ruiz-Molina, J. Veciana, J. Mater. Chem. 14 (2004) 2713.
[11] S.R. Batten, K.S. Murray, Coord. Chem. Rev. 246 (2003) 103.
[12] L. Carlucci, G. Ciani, D.M. Proserpio, Coord. Chem. Rev. 246 (2003) 247.
[13] M. Eddaoudi, D.B. Moler, H.L. Li, B.L. Chen, T.M. Reineke, M. O'Keeffe, O.M. Yaghi, Acc. Chem. Res. 34 (2001) 319.
[14] T.M. Reineke, M. Eddaoudi, M. O'Keeffe, O.M. Yaghi, Angew. Chem., Int. Ed. 38 (1999) 2590.
[15] H. Li, M. Eddaoudi, M. O'Keeffe, O.M. Yaghi, Nature 402 (1999) 276.
[16] O.R. Evans, Z.Y. Wang, R.G. Xiong, B.M. Foxman, W.B. Lin, Inorg. Chem. 38 (1999) 2969.
[17] L. Pan, X.Y. Huang, J. Li, Y.G. Wu, N.W. Zheng, Angew. Chem., Int. Ed. 39 (2000) 527.
[18] C. Janiak, T.G. Scharmann, P. Albrecht, F. Marlow, R. Macdonald, J. Am. Chem. Soc. 118 (1996) 6307.
[19] B.O. Patrick, C.L. Stevens, A. Storr, R.C. Thompson, Polyhedron 22 (2003) 3025.
[20] C.J. Oconnor, C.L. Klein, R.J. Majeste, L.M. Trefonas, Inorg. Chem. 21 (1982) 64.
[21] L. Mao, S.J. Rettig, R.C. Thompson, J. Trotter, S.H. Xia, Can. J. Chem. 74 (1996) 433.
[22] X.H. Li, Q. Shi, M.L. Hu, H.P. Xiao, Inorg. Chem. Commun. 7 (2004) 912.
[23] J.Z. Zou, Z. Xu, W. Chen, K.M. Lo, X.Z. You, Polyhedron 18 (1999) 1507.
[24] R. Kitaura, K. Fujimoto, S. Noro, M. Kondo, S. Kitagawa, Angew. Chem., Int. Ed. 41 (2002) 133.
[25] T.K. Maji, K. Uemura, H.C. Chang, R. Matsuda, S. Kitagawa, Angew. Chem., Int. Ed. 43 (2004) 3269.
[26] M. Kondo, T. Okubo, A. Asami, S. Noro, T. Yoshitomi, S. Kitagawa, T. Ishii, H. Matsuzaka, K. Seki, Angew. Chem., Int. Ed. 38 (1999) 140.
[27] J.H. Yang, S.L. Zheng, X.L. Yu, X.M. Chen, Cryst. Growth Des. 4 (2004) 831.
[28] G. Smith, A.N. Reddy, K.A. Byriel, C.H.L. Kennard, J. Chem. Soc., Dalton (1995) 3565.
[29] B.S. Zhang, Chin. J. Struct. Chem. 24 (2005) 478.
[30] R. Matsuda, R. Kitaura, S. Kitagawa, Y. Kubota, T.C. Kobayashi, S. Horike, M. Takata, J. Am. Chem. Soc. 126 (2004) 14063.
[31] J.Y. Lu, Z.H. Ge, Inorg. Chim. Acta 358 (2005) 828.
[32] C.F. Wang, E.Q. Gao, Z. He, C.H. Yan, Chem. Commun. (2004) 720.

[33] R. Cao, Q. Shi, D.F. Sun, M.C. Hong, W.H. Bi, Y.J. Zhao, Inorg. Chem. 41 (2002) 6161.
[34] J.X. Chen, S.X. Liu, E.Q. Gao, Polyhedron 23 (2004) 1877.
[35] Y. Ma, Y.K. He, Z.B. Han, Acta Crystallogr., Sect. E 62 (2006) M2528.
[36] J.Y. Lu, Coord. Chem. Rev. 246 (2003) 327.
[37] Y. Kubota, M. Takata, R. Matsuda, R. Kitaura, S. Kitagawa, K. Kato, M. Sakata, T.C. Kobayashi, Angew. Chem., Int. Ed. 44 (2005) 920.
[38] M. Gryz, W. Starosta, J. Leciejewicz, J. Coord. Chem. 58 (2005) 931.
[39] P. Richard, D.T. Qui, E.F. Bertaut, Acta Crystallogr., Sect. B 30 (1974) 628.
[40] X.M. Lin, L. Chen, H.C. Fang, Z.Y. Zhou, X.X. Zhou, J.Q. Chen, A.W. Xu, Y.P. Cai, Inorg. Chim. Acta 362 (2009) 2619.
[41] W. Starosta, J. Leciejewicz, Acta Crystallogr., Sect. E 68 (2012) M75.
[42] L.G. Zhu, S.R. Fan, Inorg. Chem. 45 (2006) 7935.
[43] N. Aliaga-Alcalde, P. Kapoor, A.P.S. Pannu, M. Sharma, M.S. Hundal, R. Kapoor, M. Corbella, J. Mol. Struct. 981 (2010) 40.
[44] C.-P. Li, M. Du, Inorg. Chem. Commun. 14 (2011) 502.
[45] P. Richard, D. Tranqui, E.F. Bertaut, Acta Crystallogr., Section B Struct. Crystallogr. Cryst. Chem. B 30 (1974) 628.
[46] H. Ptasiewicz-Bak, J. Leciejewicz, Pol. J. Chem. 73 (1999) 1887.
[47] M. Olczak-Kobza, Thermochim. Acta 366 (2001) 129.
[48] M.S. Nair, S. Jawaharunnissa, L. Kamakshi, M.S. Pillai, Indian J. Chem. A 29 (1990) 581.
[49] O.Z. Yesilel, G. Gunay, A. Mutlu, H. Olmez, O. Buyukgungor, Inorg. Chem. Commun. 13 (2010) 1173.
[50] H. Erer, O.Z. Yesilel, C. Darcan, O. Buyukgungor, Polyhedron 28 (2009) 3087.
[51] O.Z. Yesilel, A. Mutlu, C. Darcan, O. Buyukgungor, J. Mol. Struct. 964 (2010) 39.
[52] O.Z. Yesilel, H. Erer, A. Mutlu, O. Buyukgungor, Polyhedron 28 (2009) 150.
[53] H. Erer, O.Z. Yesilel, O. Buyukgungor, Polyhedron 29 (2010) 1163.
[54] O.Z. Yesilel, H. Erer, O. Buyukgungor, Inorg. Chem. Commun. 12 (2009) 724.
[55] O.Z. Yesilel, A. Mutlu, O. Buyukgungor, Polyhedron 28 (2009) 437.
[56] A.T. Colak, F. Colak, D. Akduman, O.Z. Yesilel, O. Buyukgungor, Solid State Sci. 11 (2009) 1908.
[57] O.Z. Yesilel, I. Ilker, O. Buyukgungor, Polyhedron 28 (2009) 3010.
[58] G.M. Sheldrick, Program for the Solution of Crystal Structures, University of Göttingen, Germany, 1997.
[59] C.F. Macrae, P.R. Edgington, P. McCabe, E. Pidcock, G.P. Shields, R. Taylor, M. Towler, J. van De Streek, J. Appl. Crystallogr. 39 (2006) 453.
[60] A.K. Rappe, C.J. Casewit, K.S. Colwell, W.A. Goddard, W.M. Skiff, J. Am. Chem. Soc. 114 (1992) 10024.
[61] S. Keskin, J. Liu, R.B. Rankin, J.K. Johnson, D.S. Sholl, Ind. Eng. Chem. Res. 48 (2009) 2355.
[62] V. Buch, J. Chem. Phys. 100 (1994) 7610.
[63] A.I. Skoulidas, D.S. Sholl, J. Phys. Chem. B 109 (2005) 15760.
[64] G. Garberoglio, A.I. Skoulidas, J.K. Johnson, J. Phys. Chem. B 109 (2005) 13094.
[65] D. Frenkel, B. Smit, Understanding Molecular Simulation: From Algorithms to Applications, second ed., Academic Press, San Diego, 2002.
[66] A.I. Skoulidas, D.S. Sholl, J. Phys. Chem. A 107 (2003) 10132.
[67] M.J. Fang, M.X. Li, X. He, M. Shao, W. Pang, S.R. Zhu, J. Mol. Struct. 921 (2009) 137.
[68] W.P. Wu, F.C. Zeng, Y. Wu, J. Peng, Acta Crystallogr., Sect. E 64 (2008) M61.
[69] A.W. Addison, T.N. Rao, J. Reedijk, J. Vanrijn, G.C. Verschoor, J. Chem. Soc., Dalton (1984) 1349.
[70] S. Konar, S.C. Manna, E. Zangrando, N.R. Chaudhuri, Inorg. Chim. Acta 357 (2004) 1593.
[71] H. Yin, S.X. Liu, J. Mol. Struct. 918 (2009) 165.
[72] T.S. Thakur, G.R. Desiraju, Chem. Commun. (2006) 552.
[73] M. Castro, J. Cruz, H. Lopez-Sandoval, N. Barba-Behrens, Chem. Commun. (2005) 3779.
[74] A.L. Spek, J. Appl. Crystallogr. 36 (2003) 7.
[75] L.F. Chena, Z. Lia, Y.Y. Qina, J.K. Chenga, Y.G. Yao, J. Mol. Struct. 892 (2008) 278.
[76] L. Infantes, J. Chisholm, S. Motherwell, CrystEngCommun 5 (2003) 480.
[77] L. Brammer, M.D. Burgard, M.D. Eddleston, C.S. Rodger, N.P. Rath, H. Adams, CrystEngCommun (2002) 239.
[78] O. Zimhony, C. Vilcheze, M. Arai, J.T. Welch, W.R. Jacobs, Antimicrob. Agents Chemother. 51 (2007) 752.
[79] O.Z. Yesilel, G. Gunay, C. Darcan, M.S. Soylu, S. Keskin, S.W. Ng, CrystEngCommun 2012 (2012) 2817.
[80] S. Silver, L.T. Phung, Annu. Rev. Microbiol. 50 (1996) 753.
[81] X.L. Wang, C. Qin, E.B. Wang, Y.G. Li, N. Hao, C.W. Hu, L. Xu, Inorg. Chem. 43 (2004) 1850.
[82] V.I. Isaeva, L.M. Kustov, Russ. J. Gen. Chem. 77 (2007).